Influence of the wear partition factor on wear evolution modelling of sliding surfaces

Lorenza Mattei and Francesca Di Puccio
Dipartimento di Ingegneria Civile e Industriale,
Università di Pisa
Largo Lazzarino 2, 56126 Pisa (ITALY)
l.mattei@ing.unipi.it (+39 0502218019), dipuccio@ing.unipi.it (+39 0502218076)

Abstract

Wear of engineering components is crucial to assess their performance during all their service life. Numerical wear models are a promising tool, cheaper and quicker than experimental tests, both to investigate wear effects and to compare design solutions. However, frequently, numerical models assume that only one body gets worn or both elements undergo the same volume loss.

This study proposes a generalization of the Archard wear law, introducing the concept of wear partition factor α to take into account a different wear behaviour of the rubbing elements of a coupling. The proposed approach is applied to the case of a cylinder sliding over a plane with different stroke amplitudes s_t. A numerical wear model has been developed in Abaqus®, exploiting the UMESHMOTION routine. Implementation procedures are described and discussed along with the model convergence. Twenty combinations of α and s_t were simulated covering the cases both of unilateral/bilateral wear and fretting/sliding wear. Results provide important indications on the evolution of wear volumes, wear profiles and contact variables with travelled distance, revealing the remarkable role of α.

The present study aims to an improved understanding and modelling of sliding wear evolution thus clarifying some critical issues slightly discussed by the literature.

Keywords: wear simulation; Archard wear law; wear partition factor; fretting; sliding wear

1 Introduction

Wear is a damaging process that affects both biological and engineering systems, from human to gear teeth, from bearings to artificial joints and so on. Indeed, wear occurs anytime two surfaces are in contact and in relative motion. Thus, two crucial issues arise about the reliability and performance of rubbing couplings: to predict how the components are damaged during their service life and to establish when they need to be replaced. In-silico wear simulations can greatly help to achieve these aims and this explains the large number of wear models available in the literature, from the simplest to the most advanced ones.

First of all, when developing a predictive wear model, it is worth observing that wear can affect only one of the contact surfaces or both of them, depending on their wear resistance. The different response can be influenced not only by the surfaces intrinsic properties (e.g. hardness and roughness) but also by the loading, kinematic and lubrication conditions. Typically, when one of the mating surfaces has a wear resistance much higher than the other one, the wear model is simplified as only one body wears out (i.e. unilateral wear). Otherwise, both surfaces get worn, and need to be modelled (i.e. bilateral wear). Generally, when surfaces with identical or similar material properties are coupled, the wear is bilateral, whilst when plastic is coupled with steel typically only the former gets worn.

Another key issue in wear modelling is the definition of a wear law, able to describe the relationship among volume loss, material properties and testing/working conditions. According to the literature, the most widespread wear law was proposed by Archard and states that the volume loss is proportional to the product of the normal contact force L_N and the sliding distance d, via a dimensional wear coefficient k, i.e.

$$V = k\, L_N\, d \tag{1}$$

Generally, Eq. (1) is applied to the entire coupling, meaning that V represents the total volume loss of the two surfaces, and k a kind of total wear coefficient. The use of a single value of k is quite common in the wear modelling literature, and entails that the contact bodies wear out the same volume or that only one of them lose material, which unfortunately is not a general case. Moreover, the adaptation of Eq.(1) to estimate separately the volume loss by each contact surface is rarely employed. In particular, as far as the wear modeling of general pin-on-flat sliding/fretting configurations are concerned, a review of the literature reveals that different wear resistances, i.e. different wear coefficients, of the articulating surfaces have been considered only in a few studies [1-3] and, to the best of our knowledge, the concept has been faced only marginally. Indeed, such studies are generally focused on the discussion of new wear models and computational strategies rather than on the effect of such a difference in wear resistances [1-3]. The only work that has recently deepened this matter [1] has compared the wear evolution of a pin-on-plate coupling for different values of the so-called "wear mode index", a parameter defined as a function of the wear coefficients of the contact pair, the sliding distance per cycle and the pin radius. The main limit of this study is that the wear coefficients are considered independent one from the other, i.e. not related to the total k. Moreover the tribological role of the wear mode index, hence also of the wear resistance, is not widely discussed; rather, it seems a tool/method to present results.

From an experimental point of view, in order to define separate Archard equations for the two bodies in contact, also separate measurements of the volume losses are required. However, frequently the wear loss is assumed to be equally distributed between the contact surfaces (single k value) even when experimental wear tests point out a significant difference between the wear volumes of the elements [4-6].

Thus, the present paper moves from a theoretical generalization of the Archard law (Eq.(1)), which is based on the introduction of a wear partition factor α. Such a factor describes how the volume loss of the entire contact pair is distributed between the two elements. Then, the novel approach is applied in a predictive wear model.

The aim of this work is to numerically investigate the wear evolution of sliding surfaces with different wear resistances. A Finite Element (FE) wear model of a sliding cylinder-on-plate configuration has been developed in a parametric form with respect to the wear partition factor α and the stroke length, s_t. Such a simple geometry has been chosen to facilitate the generalization of the present approach to more complex applications. Twenty combinations of α and s_t have been simulated, covering the cases of both unilateral and bilateral wear, also with different wear resistances, and both sliding and fretting wear, depending on the stroke length. The sensitivity of the wear evolution to α and s_t has been investigated by comparing the wear profiles and contact pressure distributions, fixing the total travelled distance. Hopefully, this study allows to achieve an improved understanding and modelling of the wear evolution thus clarifying some critical issues slightly discussed by the literature.

The organization of the manuscript is as follows. The background section introduces the Archard wear law in its more common form and its implementation in Abaqus according to two basic procedures. Then the case study on which the paper is focused is described. In the method section, the concept of the wear partition factor, through the generalization of the Archard law, is introduced. Secondly, the FE wear model and the simulation cases described. Third, the specific features of the wear model implementation adopted for the selected case study are reported. Finally, the results and discussion section is organized in several subsections describing: i) the numerical convergence of the model, assessed on the basis of the sensitivity analysis to both mesh and simulation parameters; ii) the main results for a reference simulated case; iii) the effect of α and s_t on the wear evolution; iv) the comparison with the literature studies.

2 Background

2.1 Archard wear law

As discussed in the introduction, the Archard wear law is commonly adopted in wear modelling using a single wear coefficient. This assumption corresponds to two special cases: only one surface wears out or

both surfaces wear of the same amount, i.e. have the same wear resistance. However, the implementation into a FE code of the Archard wear law requires further steps as the form in Eq.(1) refers to a translational relative motion between the coupling elements, under constant load. In general, we need to simulate a more complex configuration, characterized by a time-varying load, a not uniform contact pressure and a generic three-dimensional kinematics. In such a case, it is convenient to re-write Eq.(1) in local form, introducing the wear depth or linear wear at a point *P* of each contact surface as

$$h(P) = k \int_{\gamma_P} p(P,s)\, ds \tag{2}$$

where s is the arc length along the travelled path γ_P at a given time instant t (i.e. $s(t)$), and $p(P,s)$ is the local instantaneous contact pressure in P at s. Thus the volume loss is obtained as

$$V = k \int_{A} \int_{\gamma_P} p(P,s)\, ds\, dA \tag{3}$$

Equations (1-3) hold both for unilateral and bilateral wear, and, additionally can be used both for the whole coupling and for each one of the bodies in contact. That can generate a misunderstanding in defining the correct value of k to be used. In particular, when both surfaces wear of the same amount, if k holds for the couple, $k/2$ should be applied for the single bodies.

In order to model a more general wear problem with contact surfaces characterized by different wear resistances, a generalization of Eqs.(1-3) is needed and will be presented in the Sec.4.1.

2.2 FE wear model in Abaqus: basic procedures

In this section the basic procedures for simulating wear evolution in Abaqus are described. Although some concepts have already been described in the literature, we prefer to present them in this section using our own approach, that will be consistent and useful also for the original part (Sec.4.3).

Abaqus FE code is considered because is one of the most widespread for numerical wear simulations [2, 7-10], but some basic steps can be found in other codes as well.

The implementation in Abaqus of a wear model is based on the interaction among the standard FE solver, the FORTRAN user subroutine UMESHMOTION (UMM) and the adaptive mesh smoothing (AMS) available in Abaqus. Indeed, wear simulation is an incremental process, which consists in the repetition of three fundamental steps (included in one single Abaqus STEP), which constitute an FE wear cycle: i) solution of the contact problem to evaluate the contact pressure and the sliding distance, executed by the standard FE solver; ii) wear computation executed by the UMM and iii) wear implementation and mesh smoothing, executed by the AMS+UMM.

Different strategies can be adopted to reduce the computational cost of a wear model, mainly depending on the type of loading history, as described in the following paragraphs.

2.2.1 Generic loading history

Let us consider a generic loading history, as shown in Fig.1. For modeling wear evolution, such history is typically discretized in n uniform increments (corresponding also to Abaqus INCREMENTs) and, for each increment i $(i=1..n)$, an FE wear cycle is performed, repeating the three steps listed above. Thus, n geometry updates are performed for describing the wear process. It can be observed that at each increment i the solution-dependent contact variables, i.e. the contact pressure p_i^κ and sliding distance s_i^κ for every contact node κ, are passed into the UMM and are used to compute the incremental wear depth Δh_i^κ obtained by discretizing Eq.(2) as follows:

$$\Delta h_i^\kappa = k \frac{\left(p_i^\kappa + p_{i-1}^\kappa\right)}{2}\left(s_i^\kappa - s_{i-1}^\kappa\right) \quad \text{with } i = 1\ldots n \tag{4}$$

where κ spans the set Ω of the nodes of the contact surfaces, while k is the wear coefficient of each one of the bodies in contact. Note that in Abaqus, s_i^κ is provided by the CSLIP contact output, which represents the relative tangential displacement of the node with respect to the counterface. It includes both rigid and elastic components although in most cases the latter are negligible. Additionally, it is worth observing that, when i=1, p_0^κ and s_0^κ refer to the contact conditions in the initial configuration, i.e. at t=0 of the loading history. Frequently, a simplified expression is also used for the incremental wear depth

$$\Delta h_i^\kappa = k\ p_i^\kappa \left(s_i^\kappa - s_{i-1}^\kappa \right) \quad \text{with } i = 1 \ldots n \tag{5}$$

but Eq.(4) should be preferred, requiring similar computational times for improved results.
Next, the geometry update is performed by moving the contact nodes in the direction normal to the surface at the node, according to the evaluated wear depth, by the AMS+UMM. Finally, the mesh domain close to the contact, i.e. the wear boxes mesh, is smoothed in order to guarantee a high quality mesh throughout the analysis, by the AMS. The cumulative wear depth $h^\kappa(\tau)$ at each contact node κ of the mating surfaces, at a given instant τ corresponding to the η-th iteration, is

$$h^\kappa(\tau) = h_\eta^\kappa = \sum_{i=1}^{\eta} \Delta h_i^\kappa \quad 0 \le \eta \le n \tag{6}$$

so that the final wear depth of the whole loading history, is obtained for η=n, i.e.

$$h_n^\kappa = \sum_{i=1}^{n} \Delta h_i^\kappa \tag{7}$$

It should be noted that the wear depth increment is intended to lie along the normal to the surface (having unit vector $\mathbf{n}_i^\kappa$), which however changes as wear proceeds modifying the geometry. Thus a vector sum, e.g.

$$\mathbf{h}_\eta^\kappa = \sum_{i=1}^{\eta} \Delta h_i^\kappa\, \mathbf{n}_i^\kappa \quad 0 \le \eta \le n \tag{8}$$

could be more suitable than the algebraic one in Eqs.(6-7) for estimating the cumulative wear depth. However, in most cases, geometry modifications vary the normal direction less than a few degrees, thus differences between scalar and vector estimates are negligible and the former are conveniently used.

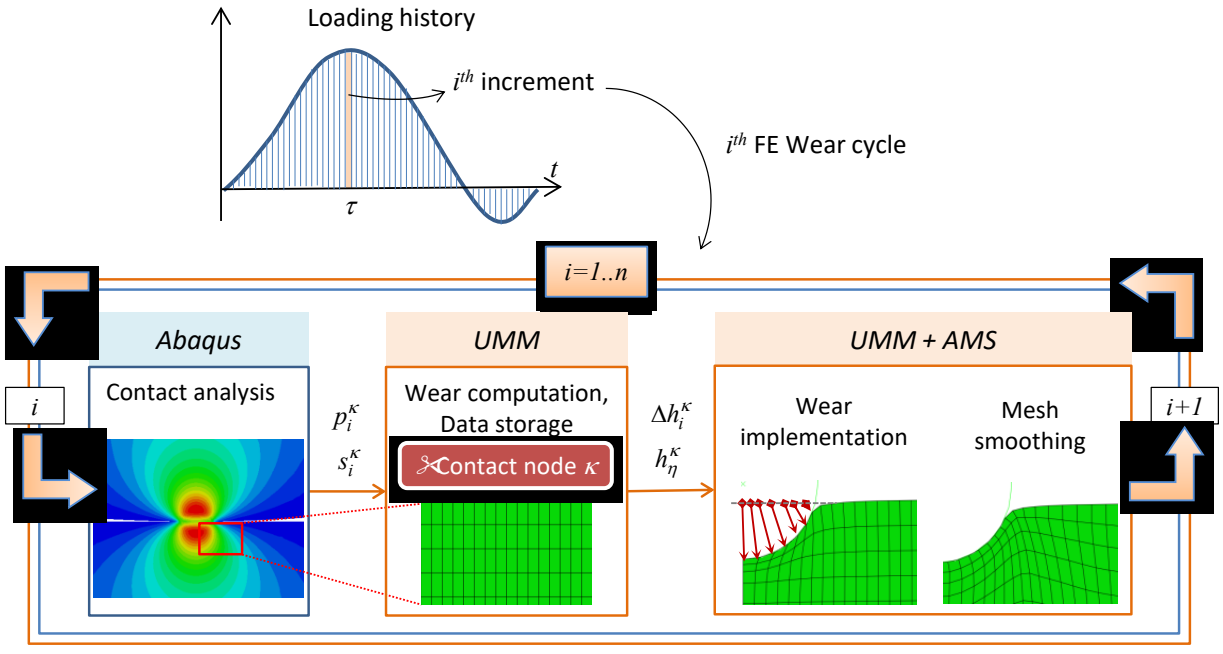

Fig.1 Generic loading history discretized in n increments (top) and scheme of the FE wear cycle repeated for each increment (bottom).

The volume loss is automatically computed by Abaqus as the change in area or volume of an element set solely due to adaptive meshing.
It is worth noting that wear computation and hence the handling/treatment of the contact variables, the implementation of the discretized Archard law in local form (Eq.(4)), as well as the storing of such variables throughout the analysis, must be coded by the user within the UMM subroutine. On the other hand, the UMM subroutine enables to easily prescribe the node motion, i.e. the wear depth, by providing a local frame that is normal to the free surface at the surface node. Also the final mesh smoothing is performed automatically by the adaptive meshing tool.

2.2.2 Cyclic loading history

Frequently, the loading history is periodic and can be described by a number N of loading cycles. Assuming that each cycle is discretized in n_c increments, adopting a quasi-continuous geometry update as in Fig.1, the whole loading history would entail $n=N\ n_c$ FE wear cycles (Fig.2), thus an equal number of contact analyses (FE runs). This can imply a high computational cost, which is the main drawback of FE wear simulation as discussed in the literature (e.g. [1, 2, 10, 11]). For example, assuming N=10000 and n_c=100, it comes n=100000 that, considering 15 s per analysis, means about 17 days for the simulation of the whole loading history.

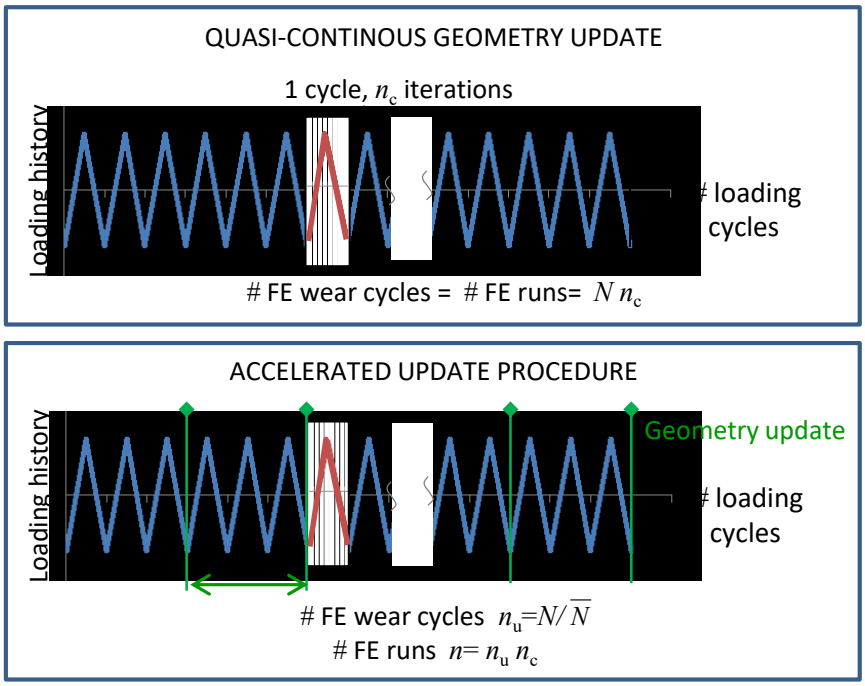

Fig.2 Cyclic loading history: quasi continuous vs. accelerated geometry update procedure.

In an attempt to reduce the computational cost, some simplifying hypotheses and computational strategies are generally adopted (e.g. [1, 2, 10, 11]), although they can implicate numerical instabilities and thus require particular attention. Most frequently (e.g. [2, 10]), it is assumed that the contact pressure is affected by the wear evolution only when the incremental wear depths become significant, that is after a critical number of loading cycles $\overline{N}$. Consequently, the geometry update (i.e. wear calculation and implementation) can be performed every $\overline{N}$ cycles, for a total of $n_u = N/\overline{N}$ times. Although a constant $\overline{N}$ is commonly used to define the critical interval for the geometry update during the whole loading history, such a number can be variable as the wear depth evolution is typically non-linear, This assumption allows to extremely reduce the computational cost, so that $\overline{N}$ is also named “acceleration factor” in [10]. However, the validity of such an assumption is worth being discussed. Firstly, the linear wear loss occurring in a single cycle is typically very low (of the order of nanometers) and does not affect the contact mechanics. On the other hand, particular attention must be given to the setting of $\overline{N}$ and n_c, since a too high value of $\overline{N}$ or too low of n_c can cause numerical instabilities related to non-smoothed worn profiles (see Sec.5.1) [10]. On

the contrary a too low value of $\overline{N}$ or too high of n_c would slow down the analysis. Consequently, a sensitivity analysis is required for the optimum choice of $\overline{N}$ and n_c.

According to the accelerated procedure, the contact analysis over the single loading cycle (without updating the geometry) is repeated within each FE wear cycle u, as shown in Fig.3. Then wear evolution is modelled in two distinct Abaqus STEPs repeated for each wear cycle u and hence for each geometry update, for a total of n_u times: the first one is devoted to the wear computation whilst the second one to the wear implementation. At each increment i (also Abaqus INCREMENT) of a wear cycle u, in the computation step the subroutine UMM is called and the contact variables $p_{u,i}^{\kappa}$and $s_{u,i}^{\kappa}$ are stored, remaining available both during and after the wear simulation. Then, at the end of each computation step, the cumulative wear depths at each contact node κ are computed according to the following relationship, obtained by replacing i with u, n with n_u and η with η_u, in Eqs.(6)

$$h_{\eta_u}^{\kappa} = \sum_{u=1}^{\eta_u} \Delta h_u^{\kappa} \quad 0 \le \eta_u \le n_u \tag{9}$$

where the incremental depth is

$$\Delta h_u^{\kappa} = k\,\overline{N} \sum_{i=1}^{n_c} \frac{\left(p_{u,i}^{\kappa} + p_{u,i-1}^{\kappa}\right)}{2} \left(s_{u,i}^{\kappa} - s_{u,i-1}^{\kappa}\right) \tag{10}$$

which stresses the role of $\overline{N}$. Frequently only pressure distribution varies with u while the sliding distance can be considered to vary only with i.

The incremental wear depths are then passed to the implementation step, which calls the UMM subroutine, to simulate wear by moving the contact nodes according to the predicted Δh_u^{κ}. Finally, the mesh smoothing is performed by AMS.

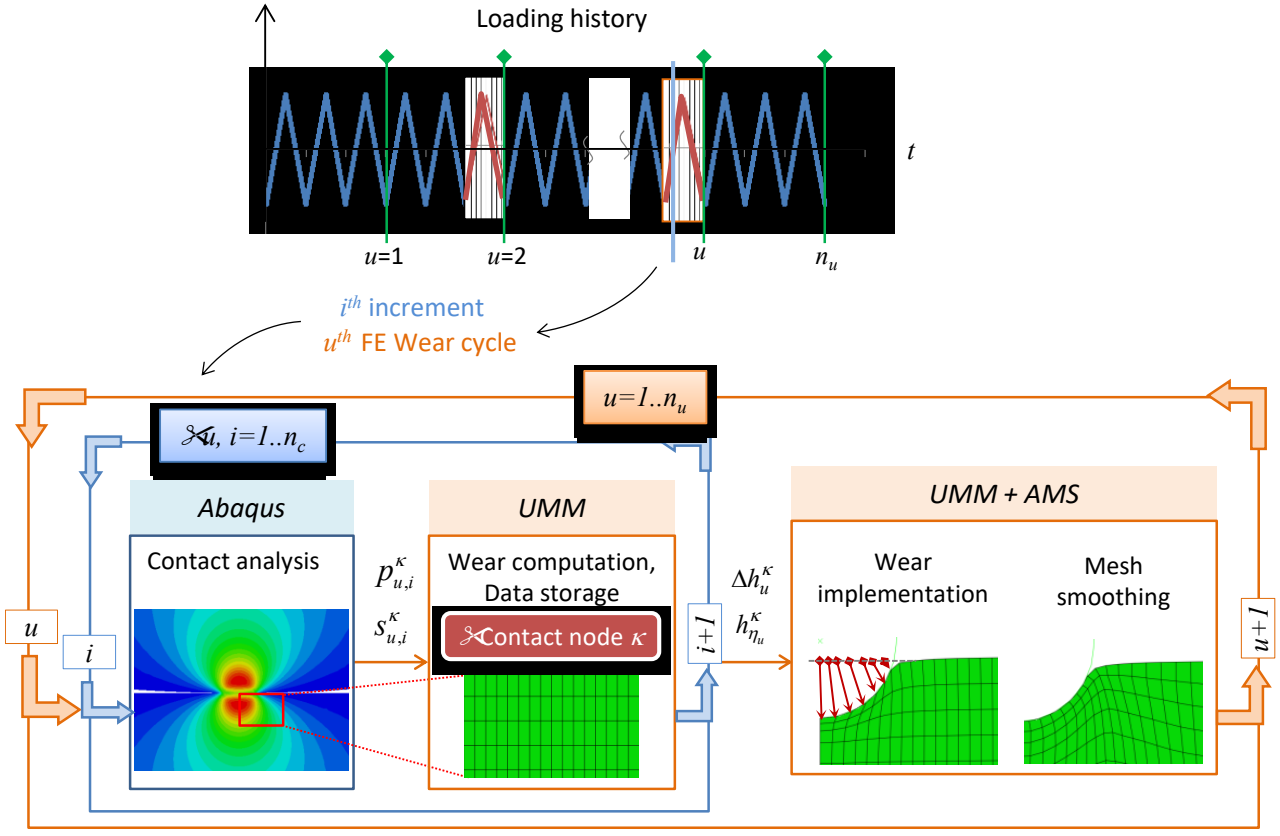

Fig.3 Flowchart of the accelerated procedure.

Further improvements in the implementation methods can be performed and those applied in the present study are described in Sec.4.3.

3 Case study: cylinder-on-plate reciprocating contact

Periodic sliding contact between non conformal surfaces represents a general problem very common in engineering applications and largely investigated in the literature both experimentally and numerically. From an experimental point of view, the following standardized wear tests are usually performed: pin-on-disc, pin-on-cylinder and pin-on-plate, with the pin geometry depending on the application (e.g. spherical, conical and cylindrical) (Fig.4). Generally, the pin is loaded and fixed while the motion is applied to the counterface as depicted in Fig.4. For the pin-on-disc/cylinder configurations, the motion is a rotation around their symmetry axis (circular sliding path), whilst for the pin-on-plate one is a reciprocating translation (linear sliding path). In fact, the reciprocating pin-on-plate arrangement can be used to investigate both the fretting and the sliding wear, which mainly differ for the sliding amplitude, being of the order of microns for the former and ranging from hundreds of microns up to tens of millimetre for the latter [12, 13]. Even the more complex contact conditions are investigated taking advantage of equivalent periodic pin-on-flat wear configurations, at least as a first step (e.g. [3]).

In the literature, the general wear problem of periodic pin-on-flat contact has been largely investigated numerically. Many numerical models implementing the Archard law are available for the tribological configurations of Fig.4. For instance pin-on-disc wear models have been proposed in [3, 14], while reciprocating sliding pin-on-plate models can be found in [1, 4, 5, 11, 15]. Some examples of fretting models for cylinder-on-plate contact are described in [2, 10, 15]. It should be noted that when the pin is spherical, the wear model is generally three-dimensional [1, 3-5, 14]; in a few cases a simplified axial-symmetric geometry is assumed [14]). On the other hand, in wear models with cylindrical pin, the analysis is restricted to a 2D plane strain case [2, 10, 11, 15]. It is worth remarking that these models generally simulate contact surfaces having the same wear coefficient [1, 3-6, 10], and only rarely different ones [1-3, 16].

In the present study a FE wear model of a cylinder-on-plate sliding contact has been developed for rubbing surfaces with different wear resistances. Moreover the model can simulate both sliding and fretting conditions, by properly setting the stroke amplitude s_t. The choice of such a case study, relatively simple, is due to several reasons: the significance of periodic pin-on-plate wear problems; the rather low computational cost; the feasibility of generalizing the proposed approach to more complex applications.

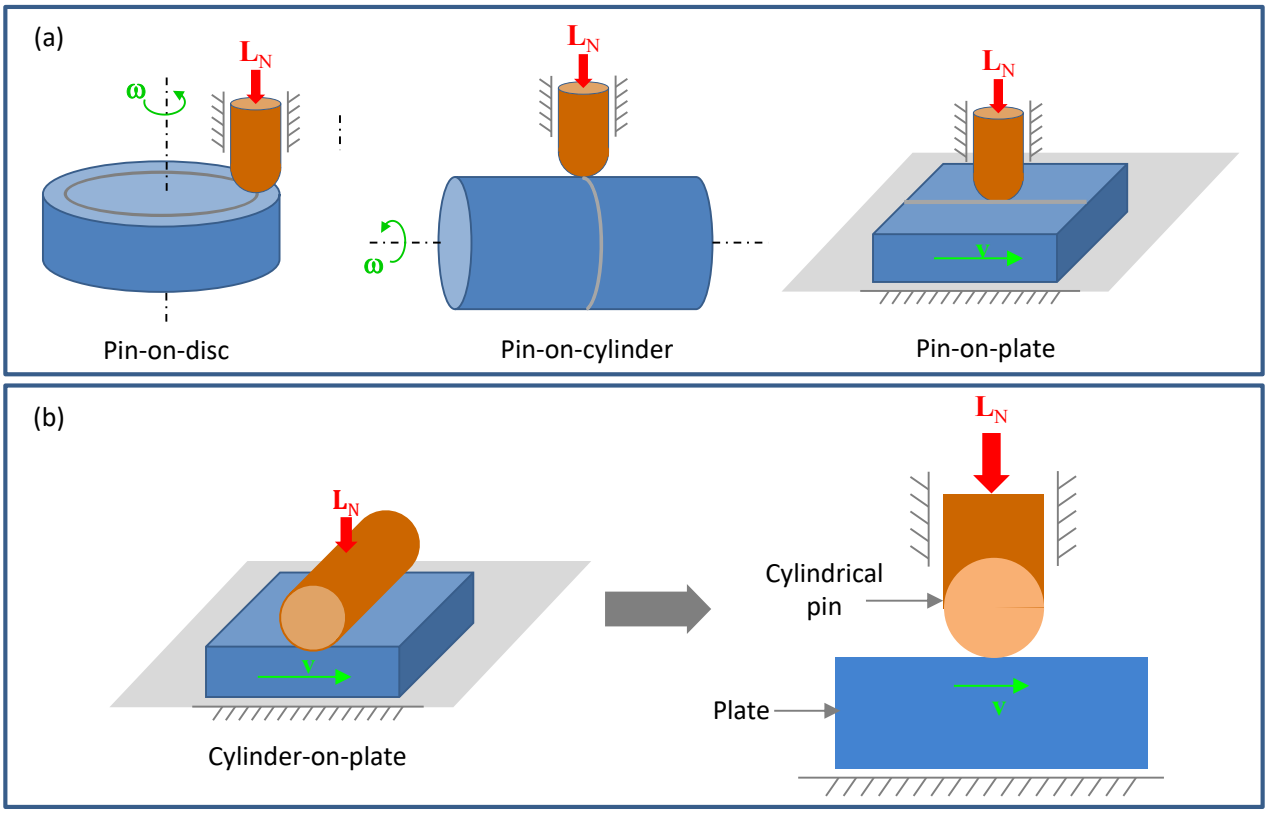

Fig.4 Sketches of the most common wear tests (a). Case study: cylinder-on-plate reciprocating contact (b).

4 Methods

4.1 Revision of the Archard law

The limitations of the Archard wear law based on a single wear coefficient have already been stressed in Sec.2.1. In order to model a general wear problem with contact surfaces characterized by different wear resistances, a generalization of Eqs.(2-10) is needed and will be proposed in the following.

First of all, a superscript b is conveniently introduced in Eq.(1) for distinguishing volumes and wear coefficients of either the two bodies in contact, in this case cylinder and plate, (i.e. b=c, p) obtaining

$$V^b = k^b L_N d \tag{11}$$

while no superscript denotes global quantities of the coupling, e.g.

$$V = k L_N d\,. \tag{1bis}$$

It is worth observing that the product $L_N d$, which denotes the work done by the frictional force divided by the coefficient of friction, is the same for the two bodies as well as for their coupling. Thus, the wear volumes V and V^b are proportional to the product $L_N d$ via their specific wear coefficient, k and k^b respectively, which represent an indicator of surfaces wear resistance, being inversely proportional to it. The values of k and k^b can be evaluated from experimental wear tests by inverting Eqs.(1,11) and measuring the volume losses V_{exp} of the couple and of the single elements according to the following

$$\begin{aligned} k &= V_{exp} \big/ (L_N d), \\ k^b &= V^b_{exp} \big/ (L_N d) \qquad b = \mathrm{c,p} \end{aligned} \tag{12}$$

In general, k^{c} and k^{p} assume different values which designate how the total wear volume is distributed between them. Similarly, the wear depth at a point P of each worn surface is given by

$$h(P^b) = k^b \int_{\gamma_{P^b}} p(P^b,s)\, ds \qquad b = \mathrm{c},\mathrm{p} \tag{13}$$

so that the volume loss of each body is obtained by integrating Eq.(13) over the articulating surface A^b

$$V^b = k^b \int_{A^b} \int_{\gamma_{\mathrm{P}^b}} p(P^b,s)\, ds\, dA \qquad b = \mathrm{c},\mathrm{p} \tag{14}$$

It should be noted that the double integral in Eq.(14) is the generalized form of the product $L_{\mathrm{N}}\, d$ so represents the work performed by the frictional force divided by the coefficient of friction. Thus, it can be also used to replace $L_{\mathrm{N}}\, d$ in Eqs.(12) for the estimation of the wear coefficients. It is worth stressing that, being the work done by internal contact forces, it can be evaluated considering P belonging to the contact surface c or p indifferently, as it holds

$$\int_{A^{\mathrm{c}}} \int_{\gamma_{\mathrm{P}^{\mathrm{c}}}} p(P^{\mathrm{c}},s)\, ds\, dA = \int_{A^{\mathrm{p}}} \int_{\gamma_{\mathrm{P}^{\mathrm{p}}}} p(P^{\mathrm{p}},s)\, ds\, dA \tag{15}$$

from which the following fundamental relationship can be derived

$$V = k \int_{A^b} \int_{\gamma_{\mathrm{P}^b}} p(P^b,s)\, ds\, dA \qquad b = \mathrm{c},\mathrm{p} \tag{16}$$

Equations (14,16) can be denoted as the generalization of the Archard wear law. Moreover, considering that

$$V = V^{\mathrm{c}} + V^{\mathrm{p}} \tag{17}$$

and combining it with Eqs. (14) and (15), we obtain

$$k = k^{\mathrm{c}} + k^{\mathrm{p}} \tag{18}$$

To the authors' best knowledge Eq. (18), despite its simplicity, is never reported in the literature. Although specific wear coefficients for the two bodies have been applied in other studies as well, the fundamental result of Eq.(18) is never mentioned or exploited, probably because the relationship in Eq.(15) was not fully developed.

As the concept of the wear coefficient k is strongly connected with the coupling more than with single elements, a dimensionless parameter α, named *wear partition factor*, is introduced in this study

$$\alpha = \frac{k^{\mathrm{c}}}{k} = 1 - \frac{k^{\mathrm{p}}}{k} \tag{19}$$

so that the volume losses can be written as

$$\begin{aligned} k^{\mathrm{c}} &= \alpha k \;\rightarrow V^{\mathrm{c}} = \alpha V \\ k^{\mathrm{p}} &= (1-\alpha) k \rightarrow V^{\mathrm{p}} = (1-\alpha)\, V \end{aligned} \tag{20}$$

The wear partition factor can span the range [0,1] assuming the values at the endpoints in case of unilateral wear and the intermediate values in case of bilateral wear. Thus, for α =0 (i.e. k^{c}=0, k^{p}= k) only the plate gets worn; moving from α=0 to α=1 the wear resistance of plate increases whilst that the cylinder

decreases, assuming the same values for α =0.5 (i.e. k^c=k^p= $k/2$); lastly, for α =1 only the cylinder is affected by wear (i.e. k^c =k, k^p =0).
The proposed approach aims at overcoming the use of a single wear factor in the Archard law, often encountered in the literature, which is ambiguous and valid only in special cases (i.e. α=0, 1 and α=0.5). Moreover it provides an original relationship between the single bodies and coupling wear coefficients.

4.2 FE model

The FE wear model was developed using the FE package Abaqus® (v. 6.11) and the UMESHMOTION (UMM) subroutine, ad-hoc coded in FORTRAN by the authors.

4.2.1 Geometry and materials

The model geometry consists in a non-conformal cylinder-on-plate coupling (Fig. 5). According to the literature [2, 10], the problem can be treated as a plane strain case, and the geometry simplified by modelling a 2D-section of the contact pair. The model consists in a half cylinder of radius R=10 mm in contact with a rectangular plate of dimensions R x 2R.

The coupling is considered a metal-on-metal one, with the following material properties for both the bodies: elastic modulus E=200 GPa and Poisson ratio ν=0.3.

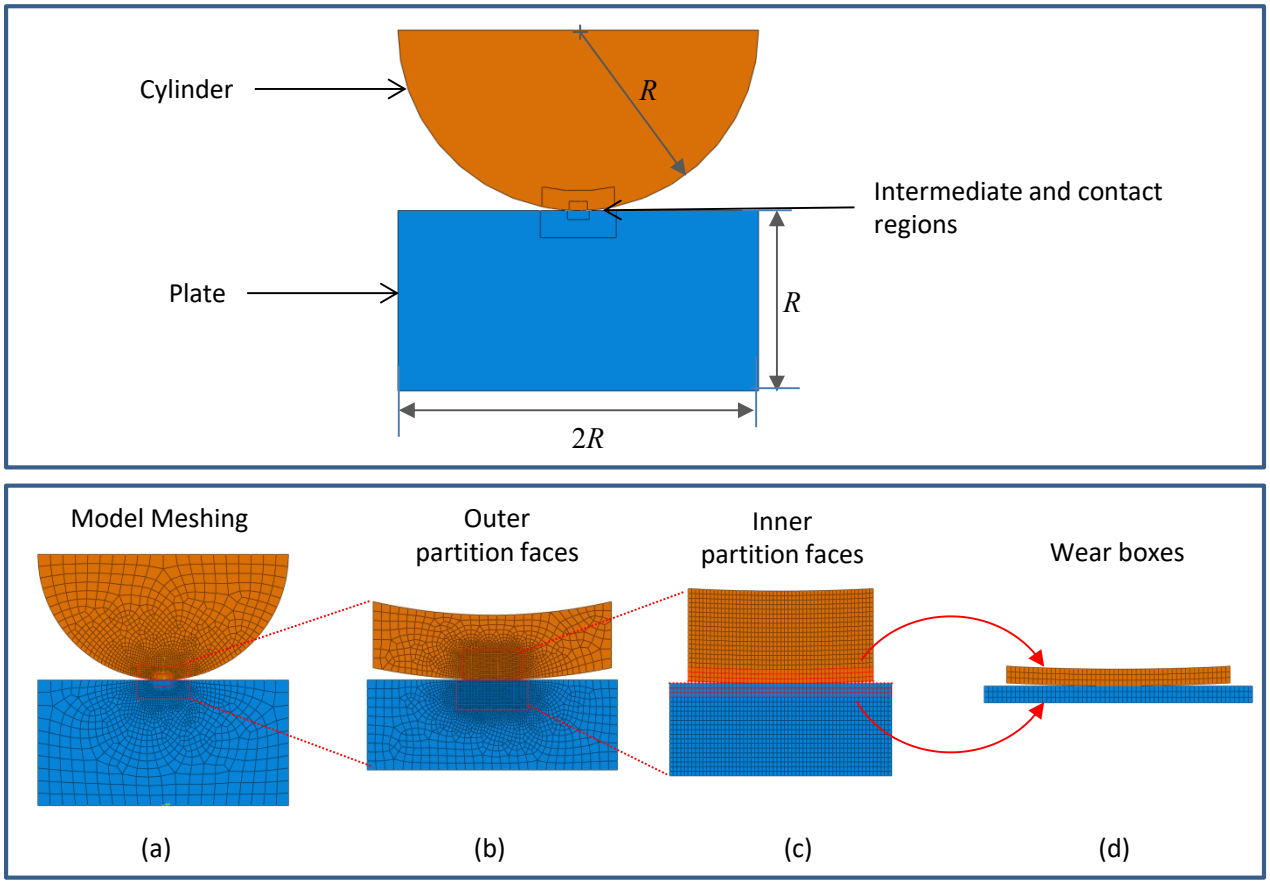

Fig. 5 Top: Model geometry and specimens dimensions (R=10 mm). The outer and inner partition faces used for meshing are also shown for each body. Bottom: Model meshing (a). Partitions faces used to optimized the meshing: zoom in the outer (b) and the inner (c) partition faces. Zoom in the wear box made of elements affected by wear (d).

4.2.2 Mesh

The model was meshed using linear plane strain elements, both triangular (CPE3) and quadrilateral (CPE4). The mesh density changes throughout the bodies, increasing in the regions adjacent the contact, where smaller elements are important to capture the sharp variations of the contact pressure. The

characteristic element size thus span from 1 mm, away from the contact, down to 20 μm, close to the contact. As a meshing technique, two partition faces, one inside the other, were defined for each part, as depicted in Fig.5. The outer and inner partition faces have dimensions respectively of about 4x1 mm and 1x0.5 mm for the cylinder, and of 4.2x1.5 mm and 1.2x0.5 mm for the plate. The meshing of the inner partitions was designed in order to ease the contact convergence and the wear implementation. In particular, the mesh is almost coincident on the contact surfaces in the configuration/position represented in Fig.5, and consists in quadrilateral elements with size of 20 μm in width and 25 μm in height. Such an element shape enables to maintain the element stability during the wear process, which indeed causes a reduction of the element height. To note that only the elements belonging to wear boxes depicted in Fig.5-d will be affected by the wear process. Each wear box consists in an element subset of the inner partitions, corresponding to the first three element rows close to the contact.

The partition sizes and the mesh densities were chosen according to the sensitivity analyses to the model mesh and the wear simulation parameters (see Sec.4.4), in order to guarantee both accuracy and low computational cost.

4.2.3 Boundary conditions

Surface interactions

The interaction between the cylinder and the plate surfaces was modelled as a frictionless and hard contact (the contact is total when is detected), taking into account the possibility of finite sliding. Additionally, a double contact was prescribed by inverting the slave and the master surfaces. That allows to obtain the nodal contact variables of both the contact surfaces, otherwise available only for the slave surface, according to the standard contact outputs of Abaqus.

The assumption of a frictionless contact is worth of being discussed. Firstly, the presence of friction in most engineering applications has a negligible effect on the contact pressure distribution [17, 18]. For instance, numerical wear investigations described in [2] and [1] and assuming a coefficient of friction of about 0.3 and 0.7, respectively, report symmetric contact pressure profiles, even during/after the wear process. Secondly, the coefficient of friction combined with stick-slip phenomena would involve further complex aspects which goes beyond the goal of the present study. However, this point is also discussed in the Results Sec.5.4.

Kinematics and loading conditions

The top of the cylinder was built-in while the kinematics of the plate was driven by the reference point *RP* of a rigid base tied at the bottom surface of the plate, as shown in Fig.6. The rotation of the rigid base was restrained while the translation in y direction was left as unconstrained since this degree of freedom was indirectly controlled by the load. The sliding contact was implemented through the motion in x direction, which consisted in a periodic reciprocating displacement as depicted in Fig.6-b. In particular, the distance travelled in a half-period is commonly known as the stroke s_t. Depending on the stroke magnitude, different wear problems can be modelled, i.e. fretting and sliding. The following values of s_t were simulated: a, $2a$ and $4a$, a being the half-width of the Hertzian contact region. A fourth kinematic condition consisted in a half reciprocating motion with $s_t = 2R$, i.e. the stroke covers the whole plate width Fig.6-b) and no return path is considered. This condition aimed at simulating the periodic motion of the pin-on-disc/cylinder tests: precisely, the two configurations for $x=\pm R$ (pin in contact with the top lateral corners of the plate) are assumed to be coincident, like whether the cylinder, after having travelled the stroke distance, would return to the initial position.

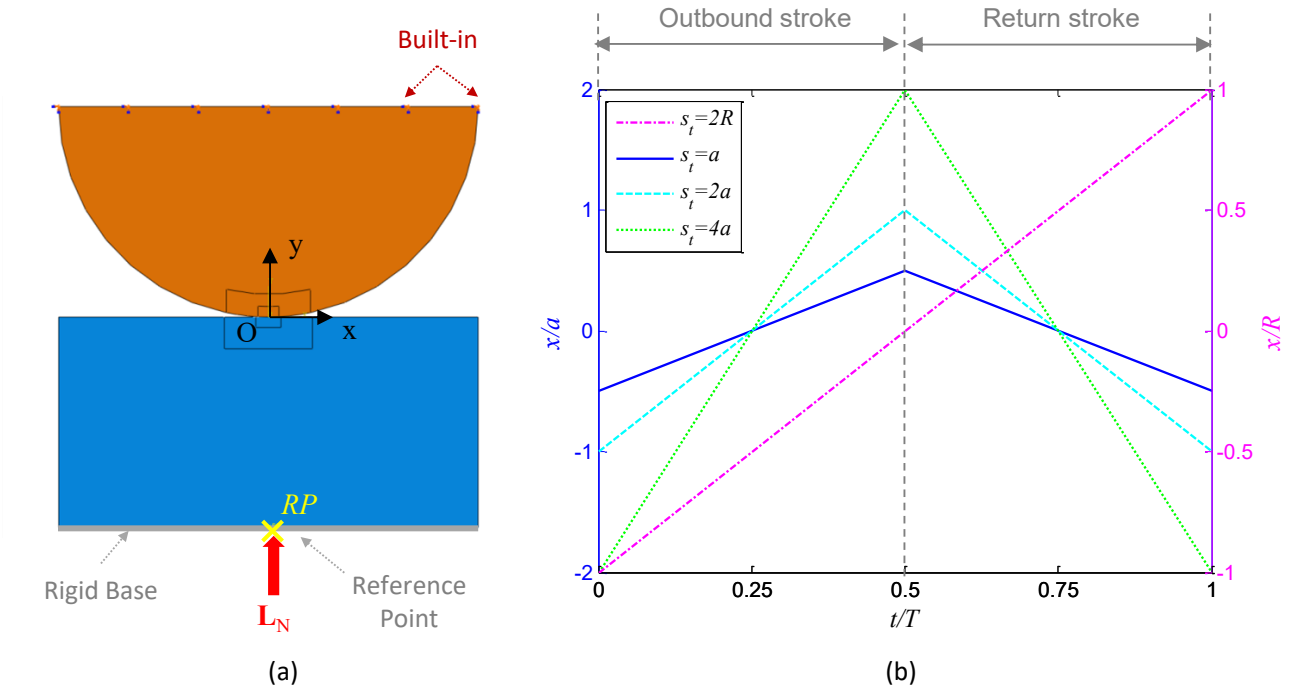

Fig. 6 (a) Scheme of the model boundary conditions. The top surface of the cylinder is built-in while the reference point *RP*, fixed to the plate, is used to apply both the kinematics and the load. The global coordinate system {O; *x*, *y*} is shown and the model is represented in its reference configuration (*x*=0). (b) Plate displacement in *x* direction vs scaled time for all simulated cases.

As far as the loading condition is concerned, a load $\mathbf{L}_N$ was applied in the *RP*, normal to the rigid base, and was kept constant throughout the wear cycle (Fig.6). A load magnitude of 100 N was adopted, which entails the following Hertzian contact conditions (unworn status): maximum contact pressure p_H=591.4 MPa, and half-width of the contact region a=0.11 mm. Thus, the simulated stroke ranged from 0.11 mm (fretting wear) to 20 mm (sliding wear), covering much different wear conditions.

It should be noted that the period of the wear cycle T is not relevant in FE wear modelling, as static simulations are carried out.

4.2.4 Simulated cases

The wear evolution was simulated for different combinations of values of the wear partition factor and stroke. In particular, α was assumed equal to 0, 0.25, 0.5, 0.75, 1 (keeping k=10^{-8} mm^2/N) while s_t=a, 2a, 4a, 2R for a total of 20 analyses. They cover the cases of both unilateral (α=0, 1) and bilateral wear (0<α<1), and both sliding (s_t=2R) and fretting conditions (s_t =a, 2a, 4a).

The sensitivity of the wear evolution to α and s_t was analysed by comparing the worn profiles and the contact pressure, on the same total travelled distance d_t=1320 mm. In the simulated cases, such a distance is covered by a different number of loading cycles, depending on the stroke, i.e.

$$N = \frac{d_t}{r\, s_t} \tag{21}$$

where r depends on the kinematic conditions and hence r=2 for reciprocating motion (s_t =a, 2a, 4a) and r=1 for half-reciprocating motion (s_t=2R).

4.3 Wear model implementation

With respect to the accelerated procedure described in Sec.2.2, in the present study the wear implementation was based on two additional computational strategies, which helped to further reduce the processing time:

a) Simulating only half loading cycle, that means $n_c/2$ increments
b) Dealing separately with cases where the worn plate surface remains plane.

a) The first simplification derives from the observation that in reciprocating contacts (for which r=2), the outbound ($0 \le t/T \le 0.5$) and the return ($0.5 \le t/T \le 1$) stroke within a wear cycle cause identical wear conditions both for the cylinder and the plate, thus only half wear cycle can be simulated. Consequently, the number of FE runs per wear cycle, i.e. of simulated increments, can be reduced to $n_c/2$ also halving the number of total FE runs $n = \overline{N}\, n_c/2$. Accordingly, the wear losses are obtained by doubling the wear predictions of the half-cycle. On the other hand, the simulation of the half-reciprocating contact (for which r=1), corresponding to the simulation of a single stroke, requires the same number of FE runs $n_c/2$ but not the doubling of the wear predictions. Consequently, Eqs.(10) and (9) are replaced by the following ones, respectively

$$\Delta h_u^{b,\kappa} = r\, k^b\, \overline{N} \sum_{i=1}^{n_c/2} \frac{\left(p_{u,i}^{b,\kappa} + p_{u,i-1}^{b,\kappa}\right)}{2} \left(s_{u,i}^{b,\kappa} - s_{u,i-1}^{b,\kappa}\right) \quad b = \mathrm{c,p} \quad r = 1,2 \tag{22}$$

$$h_{\eta_u}^{b,\kappa} = \sum_{u=1}^{\eta_u} \Delta h_u^{b,\kappa} \quad 0 \le \eta_u \le n_u, \quad b = \mathrm{c,p} \tag{23}$$

where the upper script b are introduced for distinguishing between the cylinder and the plate, whose wear coefficients are related to the partition factor according to Eq.(20). As mentioned in Sec.2.2, when i=1 the quantities $p_{u,0}^{b,\kappa}$ and $s_{u,0}^{b,\kappa}$ describe the contact conditions at the beginning of the wear cycle u and hence at the beginning of the correspondent loading cycle, i.e. in x=-s_t/2. In particular, at the first wear cycle u=1, i.e. in the unworn conditions, $p_{1,0}^{b,\kappa}$ corresponds to the Hertzian pressure and the sliding distance $s_{1,0}^{b,\kappa}$ is due only to the elastic deformations.

b) A subset of cases has been identified for which the plate surface remains flat throughout the wear process and consequently the contact analysis does not vary within the loading cycle. Therefore, the wear predictions do not require the simulation of the sliding motion of the plate and only one FE run for loading cycle has to be performed (n_c=1). That happens when the plate does not wear (i.e. α=1 and $\forall\, s_t$) or wears uniformly, i.e. in case of sliding contact (i.e. s_t=2R, $\forall\, \alpha$). In such cases, the wear depth at each node of the cylinder contact surface at any wear cycle u can be obtained as

$$\Delta h_u^{\mathrm{c},\kappa} = r\, \alpha\, k\, \overline{N}\, p_{u,1}^{\mathrm{c},\kappa} \left(s_u^{\mathrm{c},\kappa} - s_{u-1}^{\mathrm{c},\kappa}\right) \tag{24}$$

Since the elastic component of the sliding distance (i.e. the sliding produced by a change in the elastic deformation caused by pressure redistribution after the geometry update) was proved to be significantly lower than s_t, the following approximation can be assumed

$$s_{u,1}^{\mathrm{c},\kappa} - s_{u,0}^{\mathrm{c},\kappa} = s_u^{\mathrm{c},\kappa} - s_{u-1}^{\mathrm{c},\kappa} \approx s_t \tag{25}$$

and thus Eq.(23) can be simplified as

$$\Delta h_u^{\mathrm{c},\kappa} = r\, \alpha\, k\, \overline{N}\, p_{u,1}^{\mathrm{c},\kappa}\, s_t \tag{26}$$

In case of sliding contact, also the uniform wear loss of the plate needed to be predicted. That was easily computed considering that, during a loading cycle, each node of the plate surface, moving below the cylinder, is subjected to every value of the contact pressure profile. Moreover the sliding distance increment Δs is given by the element size of the wear box elements. Thus, the uniform wear depth of the plate surface generated in a wear cycle u results proportional to the integral of the contact pressure over the contact surface, according to the following equation

$$\Delta h_u^{\mathrm{p},\kappa} = (1-\alpha)\, k\, \overline{N}\, \Delta s \sum_{\kappa} \frac{(p_{u,1}^{\mathrm{p},\kappa} + p_{u,1}^{\mathrm{p},\kappa+1})}{2} \quad if\ r=1 \tag{27}$$

where the nodes κ and κ+1 belong to the same element and thus the counter κ allows to span over the contact region, moving from one element to the closest one.

Therefore, two procedures were implemented in two different subroutines, differing for simulating (procedure *SP*) or not (procedure *NSP*) the sliding motion of the plate.

The global flow-chart is provided in Fig.7. It can be noted that both procedures have as input the two analysis parameters α and s_t and the total travelled distance to be simulated, i.e. d_t. First, a check is performed on their values (s_t =2R, α=1 or not) to select the execution of the *SP* or *NSP* procedures. Then, such inputs are used to set r and to compute N (from Eq.(21)) and the number of wear cycles n_u, exploiting the values of $\overline{N}$ and n_c estimated by the sensitivity analyses.

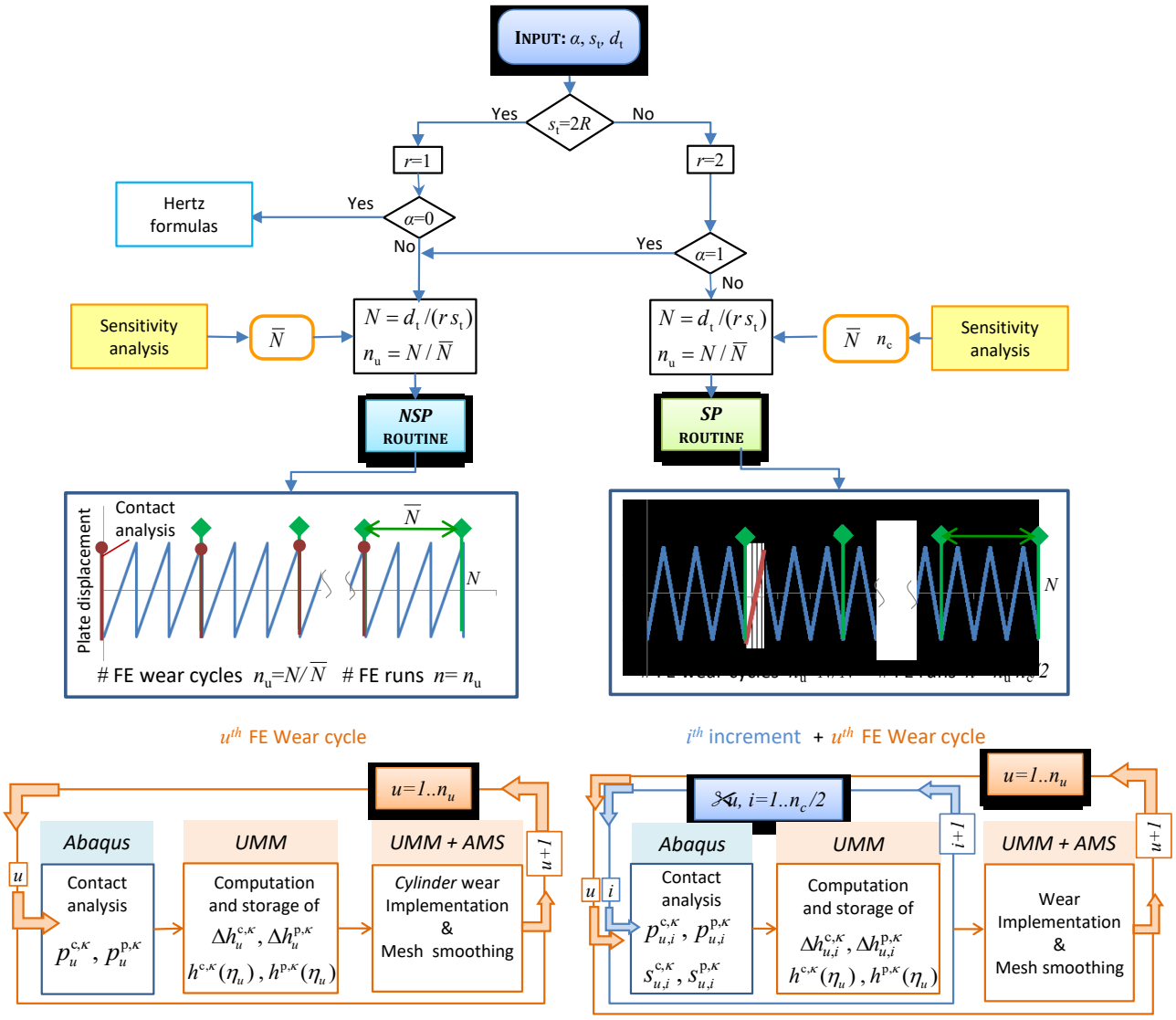

Fig. 7 Flow-chart of the implementation procedures *SP* and *NSP*.

As shown in Fig.7, the NSP procedure resembles the quasi-continuous implementation (Fig.2), as each wear cycle corresponds to a contact analysis and successive geometry update. However, in this case the increment is defined by u instead of i as in Fig.1. It is worth mentioning that the geometry update of the plate is not implemented in the FE model because the worn plate remains a flat surface. It can also be noted that the case α=0 (within the NSP procedures) under sliding contact does not require any FE simulation as

the geometry is not affected by wear and the contact problem can be solved analytically by means of Hertz formulas.

On the other side, the SP procedure is analogous to the one described in Fig.3 for the accelerated procedure, apart from the values of some indexes and superscripts. In particular the index i varies in the range $1...n_c/2$, according to the above simplifications, and specifications for the two bodies are introduced as in Eqs.(22-23).

4.4 Model convergence requirements

The numerical convergence of the wear model required two sensitivity analyses, one for the unworn configuration and the other one for the worn configuration. The former consisted in the classical mesh sensitivity analysis, according to which the mesh element size is repeatedly halved until the maximum contact pressure remains almost unchanged. In particular, the mesh size was reduced until the maximum contact pressure differed less than 1% with respect to the Hertzian solution p_H.

The sensitivity analysis for the worn configuration dealt with the optimal setting of the parameters for model implementation, i.e. $\bar{N}$ and n_c for the procedure *SP* and just $\bar{N}$ for the procedure *NSP*. The analysis was carried out for each simulation case of Sec.4.2.4 because both $\bar{N}$ and n_c are affected by the simulated conditions. It consisted in refining initial values of $\bar{N}$ and n_c until the predicted worn profiles after 10-20 geometry updates were smooth and symmetrical for both components. In particular, the initial guess value of $\bar{N}$ was chosen so that the initial total (cylinder + plate) wear depth increment Δh_0, defined as

$$\Delta h_0 = \bar{N}\, k\, p_H\, 2 s_t \tag{28}$$

was about 0.1 μm. It is worth noting that Δh_0 is an overestimation of the maximum total wear depth to be implemented at the first wear step (i.e. at the first geometry update). On the other hand, the initial value of n_c was set in order to guarantee each surface node to keep the contact throughout two consecutive increments. Since interplay exists between $\bar{N}$ and n_c, once their initial values were defined, a trial and error procedure was necessary to evaluate the couple of optimized values of $\bar{N}$ and n_c, which guaranteed the model convergence. The results of the sensitivity analysis for the worn configuration are summarized in Table 1. They revealed that optimum value of n_c was the same for all simulated cases, i.e. n_c=100, whilst $\bar{N}$ depended on the simulated conditions and thus on Δh_0.

The computational times vary significantly with the simulated case and hence with the implementation procedure, spanning the interval 1 min – 100 min on an Intel Xenon processor at 3.19 GHz and 8 GB RAM. In particular, simulations adopting the *SP* procedure typically require 60-100 min depending on the value of $\bar{N}$ (as n_c=100 for all cases), whilst those one exploiting the *NSP* procedures take less than 2 min 30 s.

Table 1 Values of $\bar{N}$ and Δh_0 for all the simulated cases, for n_c=100. For each stroke (*a, 2a, 4a 2R*), its length and the number of cycles *N* are reported.

		s_t							
		a (0.11 mm, N=6000 c)		*2a* (0.22 mm, N=3000 c)		*4a* (0.44 mm, N=1500 c)		*2R* (20 mm, N=66 c)	
		$\bar{N}$	Δh_0 (μm)	$\bar{N}$	Δh_0 (μm)	$\bar{N}$	Δh_0 (μm)	$\bar{N}$	Δh_0 (μm)
α	0	75	0.1	50	0.13	30	0.15	--	--
	0.25	100	0.13	40	0.1	25	0.13	1	0.12
	0.5	100	0.13	50	0.13	30	0.15	1	0.12
	0.75	100	0.13	40	0.1	20	0.1	1	0.12
	1	100	0.13	50	0.13	30	0.15	1	0.12

5 Results and discussion

The main outputs of both procedures consist in the evolution of the pressure and wear profiles of the two bodies in contact. Such profiles are obtained extracting the contact/wear variables along node paths in undeformed configuration and with the node distance scaled by a. In particular, wear profiles are obtained by subtracting the computed wear depth from the original geometry since it was verified that the difference with respect to the real wear profile (i.e. considering the vector expression of the wear depth in Eq.(8)) is negligible (lower than 0.1%).

5.1 Model convergence analysis

The convergence analysis for the worn configuration is a fundamental step when developing a wear model, since a precise setting of the implementation parameters allows to reduce the computational costs, preserving accurate results. In order to clarify the important role played by the implementation parameters $\overline{N}$ (for *SP* and *NSP*) and n_c (for *SP*) on the reliability of the predictions, an example of convergence analysis is provided for the case $s_t=a$ and α=0.5, at N=1000. In particular, the effect of different combinations of $\overline{N}$ and n_c values on pressure and wear profiles is described in Fig.8: in a) for n_c=40 while $\overline{N}$ =50, 100, 200; in b) for n_c=200 while $\overline{N}$ =50, 100, 200 and in c) $\overline{N}$ = 100 and n_c=16, 40, 100, 200. Figure 8-a shows that the convergence was not reached for n_c=40 as the pressure and worn profiles presented numerous irregularities and, in particular, characteristic pressure peaks increased towards the contact borders. Such an effect was due to numerical instabilities caused by a too high $\overline{N}$, as also reported in the literature [2, 10]. Moreover, both the pressure and the wear profiles resulted asymmetric with respect the y-axis, which is in disagreement with the symmetry of the problem. Such an effect, clearly showed in the plate worn profiles was caused by a too low value of n_c, in fact the increase of n_c up to 200 led to the disappearance of such asymmetries (Fig.8-b). Moreover, assuming $\overline{N}\leqslant$100 (with n_c=200), the model convergence was reached and smooth and symmetric profiles both of contact pressure and worn geometry were predicted (Fig.8-b). To the purpose of reducing as much as possible the computational cost, a sensitivity analysis with respect to n_c was also carried out fixing $\overline{N}$=100, and thus the optimized couple of input parameters $\overline{N}$=100 and of n_c=100 was evaluated (Fig.8-c). The effect of a decreasing n_c, i.e. asymmetric profiles, is also highlighted in Fig. -c.
The sensitivity analysis showed that the effect of non-convergent simulation parameters, and in particular of n_c, affected plate wear predictions more significantly than pin ones. That can be explained considering that the contact regions continuously change for the plate, moving over the plate surface, whilst are almost constant for the pin, and thus the effect of the stroke discretization results enhanced for the plate.

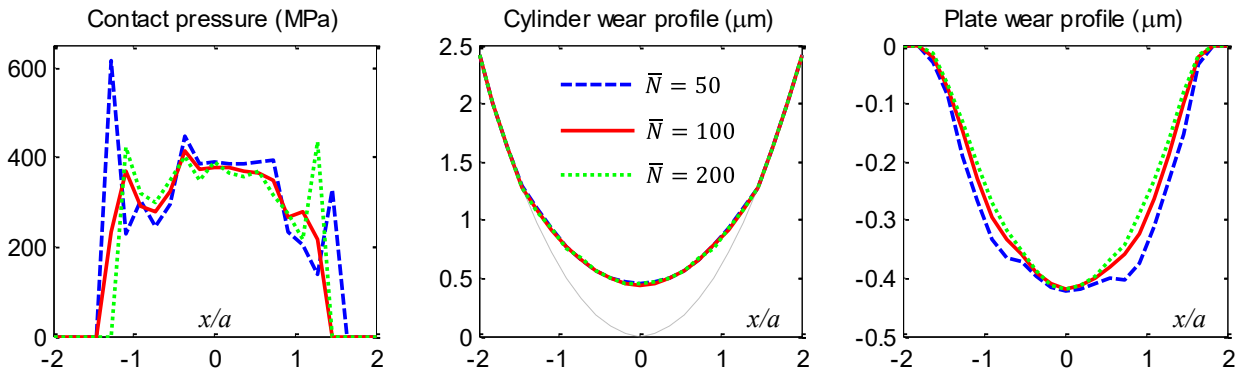

(a) n_c=40 and $\overline{N}$ = 50, 100, 200

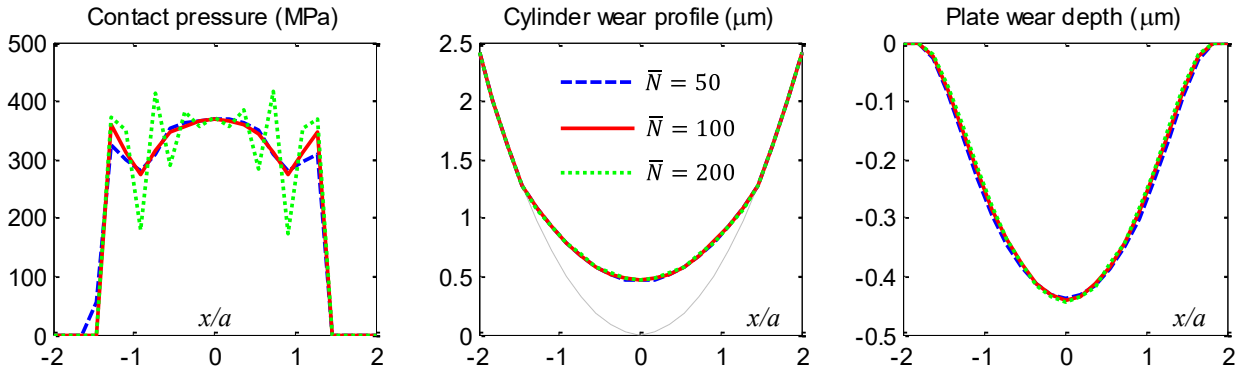

(b) n_c=200 and $\bar{N}$ = 50, 100, 200

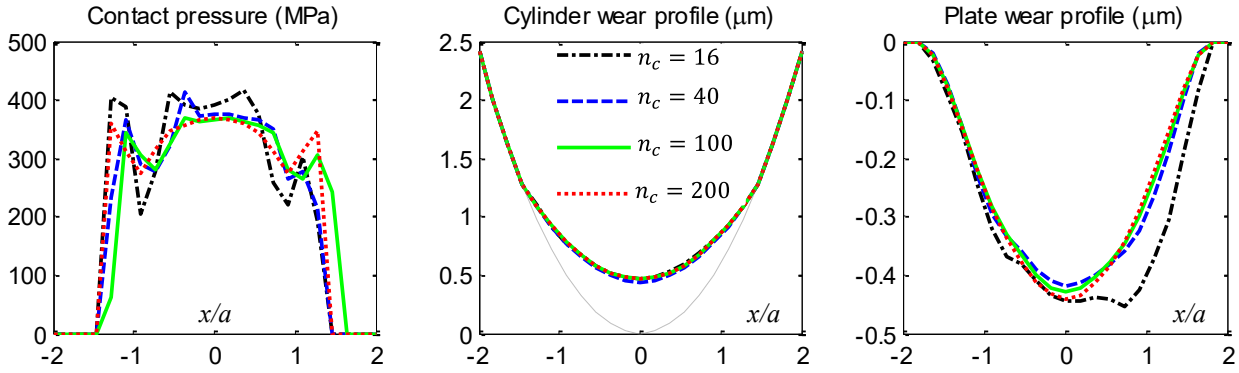

(c) $\bar{N}$ =100 and n_c=16, 40, 100, 200

Fig. 8 Effect of the different combinations of values for $\bar{N}$ and n_c on the pressure and wear profiles predicted for the case s_t=a and α=0.5, at N=1000.

5.2 General features of the wear evolution in sliding surfaces

The main results for each simulation case consists in the evolution of the contact pressure and wear profiles with increasing wear cycles; as the number of the loading cycles N is different from case to case (Table 1) results are plotted with respect to the travelled distance d

$$d = u\,\bar{N}\,r\,s_t \quad u = 1 \ldots n_u \tag{29}$$

whose total value has been fixed at d_t=1320 mm for all simulations (see Eq.(21)). Other important results are the trends of the maximum wear depth both of pin h^c_{max} and plate h^p_{max}, the wear volumes and the maximum contact pressure at the centre of the contact area, labelled p_{max}. Although in some cases higher peak values were located at the borders of the worn regions, we chose to describe p_{max}, that is how the maximum value of the Hertzian solution changes with wear evolution, instead of the real maximum contact pressure at each increment.

Some typical features of the wear process which are common to all simulated cases can be pointed out. Thus, as an example, the results for s_t=a and α=0.5 are considered and discussed in the present section. At the first wear cycle, when the Hertzian solution holds, the contact region with an amplitude of 2a translates of s_t=a over the plate surface, resulting in worn areas almost equal to 2a and 3a for the cylinder and the plate, respectively (Fig.9-a,b). As wear proceeds, a wear scar on the cylinder and a wear groove on the flat surface develop (Fig.9Fig. -a,b): the coupling surfaces become more conforming, the contact/worn areas widen and, consistently, the contact pressure flattens (Fig.9-c). It is worth noting that the contact pressure profile presents characteristic peaks at the contact edges due to the discontinuity of curvature radius at the borders between the worn and unworn regions, both on pin and plate surfaces. However, such peaks tend to reduce with increasing wear cycles (Fig.9-c). The maximum contact pressure markedly lowers (about 66%) as wear develops, although the maximum wear depths reach roughly 2 μm. While h^c_{max} and h^p_{max},

increase not linearly with time, the trend of the wear volume is perfectly linear. These general characteristcs of the wear process are well consistent with the literature (e.g. [1, 2, 10, 15]).

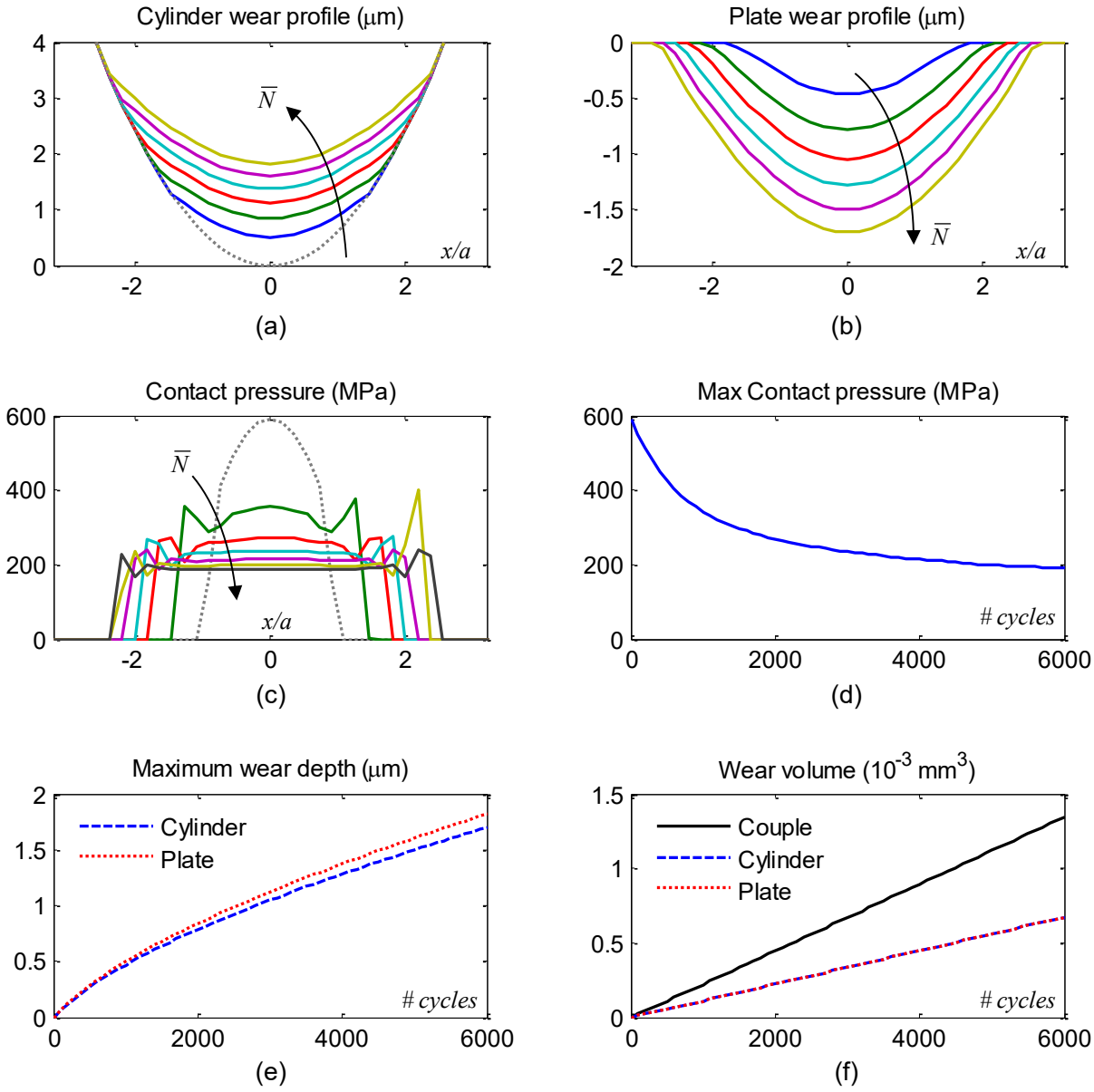

Fig. 9 Main results of the case $s_t=a$ and $\alpha=0.5$. The effect of the wear evolution over 6000 cycles is described in terms of: cylinder (a) and plate (b) wear profiles; contact pressure distribution (c); trends of maximum contact pressure (d), maximum wear depths (e) and wear volumes during the loading history.

Additionally, it should be noted that the same value of the total wear volume is predicted for all the 20 simulated cases, that is 1.320 10^{-3} mm^3, according to Eq.(1). The partition factor α distributes the total wear volume between the bodies but also the single volume losses remain obviously linear and do not dependent on the stroke amplitude, but on α and on the total travelled distance d.

5.3 Effect of the wear partition factor and the stroke amplitude on wear evolution

This section describes the results of the sensitivity analysis of wear evolution with respect to the wear partition factor and the stroke amplitude, for the twenty combinations of α and s_t described in Table 1.

5.3.1 Effect of the wear partition factor

All simulations pointed out that the wear partition factor α plays a fundamental role on the wear evolution of sliding surfaces, affecting wear rates, wear profiles and contact pressure. The redistribution of the total wear volume between the mating surfaces is well depicted in Fig.10, where the worn profiles both of cylinder and plate are compared for different values of α and s_t. The main effects of α appear to be independent from the stroke amplitude and, moving from α=0 (no wear of the pin) to α=1 (no wear of the plate), the pin wear scar increases both in width and depth, whilst the plate wear groove becomes less marked. This opposite trend of pin and plate wear losses vs. α is also demonstrated in Fig.11 (left and central columns), which shows the maximum linear wear of the contact bodies as a function of the travelled distance d.

As far as the contact pressure is concerned, Fig.10 shows that the higher the value of α (i.e. the deeper the cylinder wear scar and thus the flatter its surface), the more conformal the contact and the more uniform the contact pressure distribution at the centre of the contact region. Additionally, the pressure peaks at the contact edges, not found for the case α=0, occur and become more marked with increasing values of α. Furthermore, as depicted in Fig.11 (right column), the maximum contact pressure significantly decreases with the travelled distance for all values of α. However, it should be noted that the effect of α on the evolution of the contact pressure is strongly affected by the stroke amplitude, resulting more significant for larger strokes. For instance, in case $s_t=a$, similar contact pressure distributions and trends of p_{max} are predicted for different values of α, as depicted in the right columns of Fig.10 and Fig.11, respectively. On the other hand, in case $s_t=2R$, much different pressure distributions are predicted for different values α, holding the Hertzian solution for α=0 and a uniform pressure distribution (at the centre of the contact) for α=1. This is also confirmed by the evolutions of p_{max} portrayed in Fig.11 (right column). Indeed, for $s_t=4a$ and α=0, p_{max} decreases almost linearly with the travelled distance, whilst, for higher values α , it decreases non-linearly dropping down in the first 500 c.

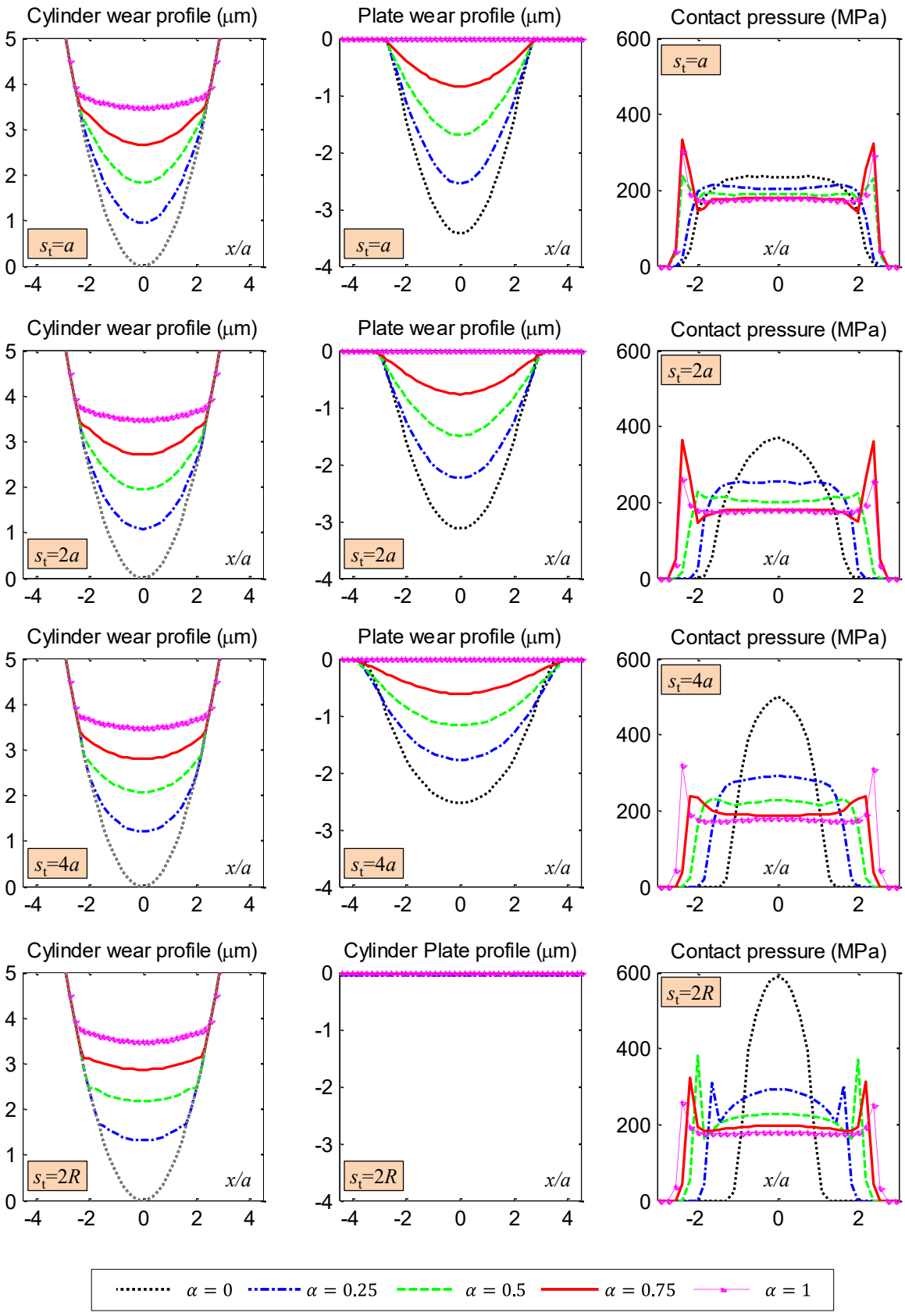

Fig. 6 Effect of the wear partition factor α on the wear evolution of sliding surfaces for d_t=1320 mm. Plots of wear profiles of cylinder (left column) and plate (central column), and of contact pressure distribution (right column). In each plot curves with different values of α (0, 0.25, 05, 075, 1) are represented. Each row gathers plots of a specific stroke amplitude s_t.

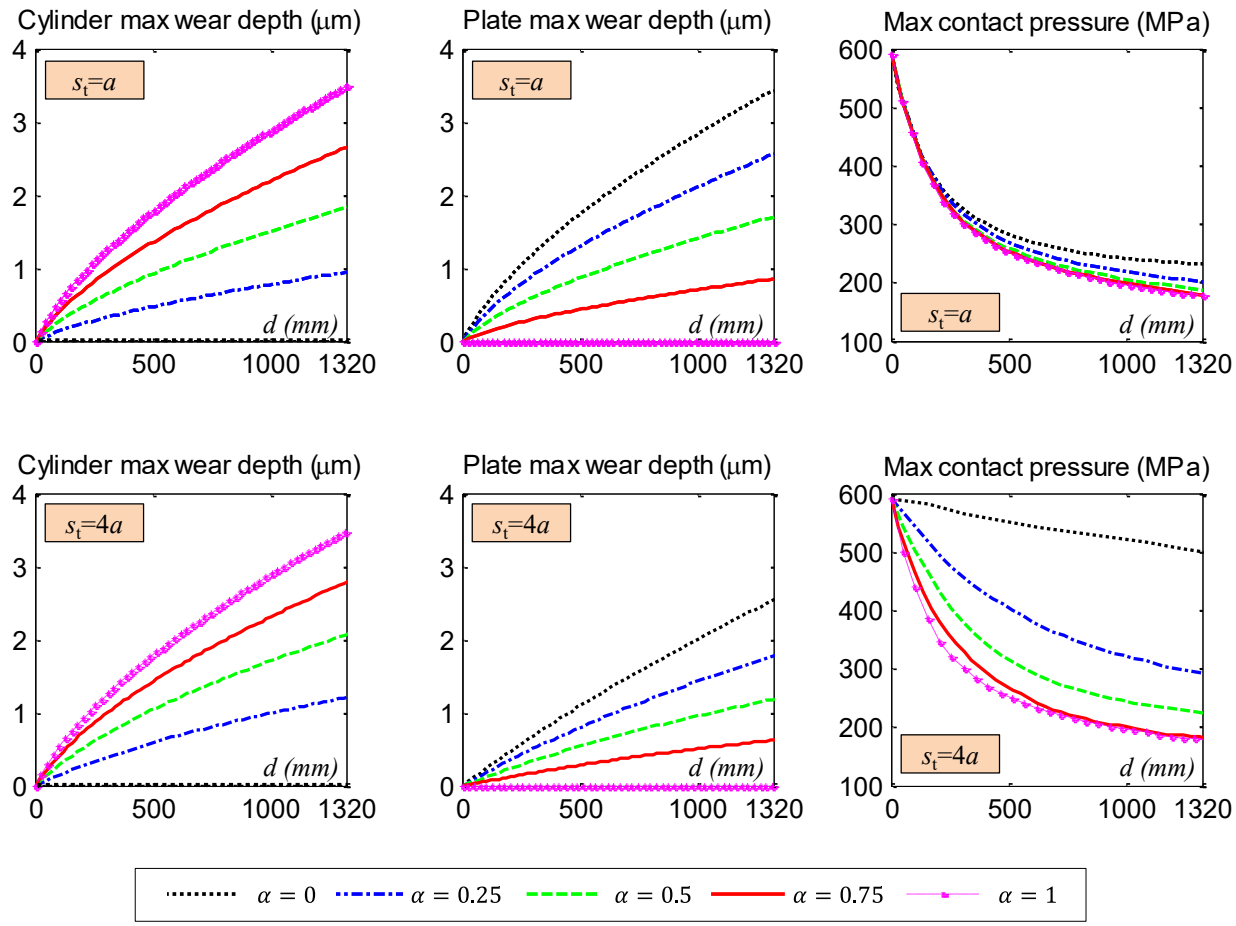

Fig. 7 Effect of the wear partition factor α on the trend of maximum wear depth of cylinder (left column) and plate (central column) and of maximum contact pressure (right column) with increasing travelled distance d: the cases s_t=a (top) and s_t =4a (bottom) are considered as examples.

5.3.2 Effect of the stroke amplitude

The effect of the wear partition factor is modulated by the stroke amplitude, as highlighted in Figs. 10-11. In order to explain more clearly such a modulation, the effect of stroke for a given α is firstly considered. In particular, Figure 12 (left-central columns) compares the wear profiles caused by different stroke amplitudes for α =0.5, showing that s_t causes a kind of wear redistribution between pin and plate. Indeed, the higher the value of s_t, the wider and less depth the wear groove on the plate, and thus the less conformal the contact and the less wide and more depth pin wear region. In the extreme case of s_t=2R, the plate surface being flat, the contact is even less conformal and such an effect is stressed.

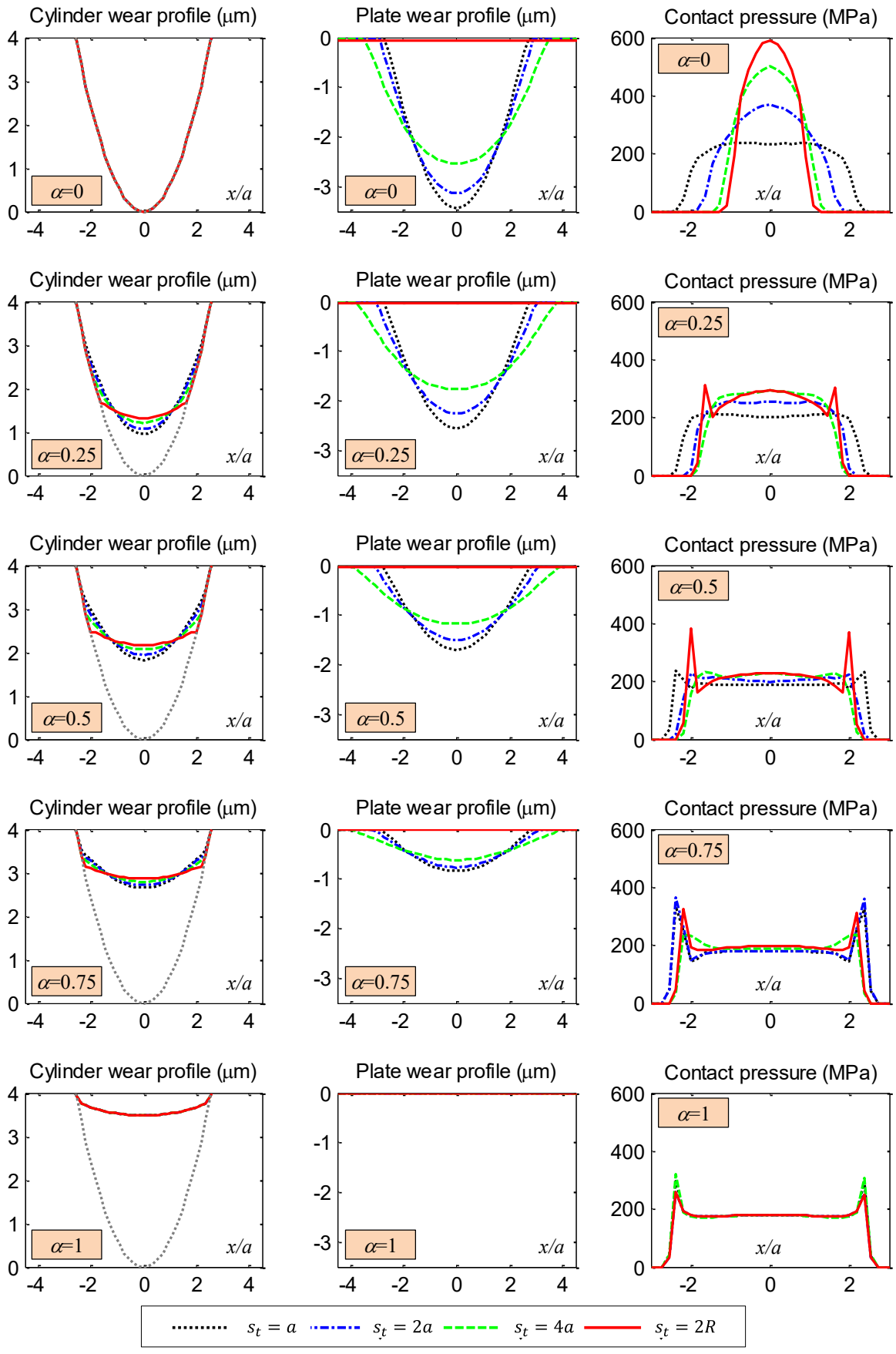

Fig. 12 Effect of the stroke amplitude on the wear profiles of cylinder (left column) plate (central column), and of contact pressure distribution (right column) for any case of α (0, 0.5, 0.25, 0.75, 1) (d_t=1320 mm). In each plot curves with different values of s_t (a, $2a$ $4a$ $2R$) are represented. Each row gathers plots of a specific wear partition factor α.

The effect of the stroke on the wear evolution can be captured also from Figs. 10-11 (left-central columns). For instance, by comparing the wear profiles of the cases $s_t=a$ and $s_t=4a$ for a given α, it can be observed that for higher values of s_t the plate worn region becomes wider and flatter, whilst the opposite happens for the pin, even if less markedly. This is also proved by the comparison of the correspondent maximum wear depth trend in Fig.11: for the same value of α, the maximum wear depth of the cylinder is higher for $s_t=4a$ than $s_t=a$, while the opposite happens for the plate.

It can be noted also that the effect of stroke amplitude is in agreement with the contact pressure distributions. For a given α, the lower the stroke, the more conformal the contact, the more uniform the contact pressure (at the centre of the contact region) (right columns of Fig.10 and Fig.12). However, such an effect is more marked for low values of α (0–0.5). Accordingly, Fig.12 shows that the pressure distributions predicted for $\alpha=1$ are almost uniform and do not vary with s_t, as well as the cylinder wear profile. Also for $\alpha=0.75$ pressure plots are very similar and uniform for any values of s_t whilst those predicted for $\alpha=0.25$ are much different. In the latter case the pressure distribution is almost uniform for low strokes, but presents a maximum value at the centre of the contact region at higher strokes. In particular, for $\alpha\to 0$ and $s_t \to 2R$, the contact pressure tends to the Hertzian solution. Additionally, it can be observed that the smaller the values of s_t and α, the lower the edge effects, i.e. lateral pressure peaks.

5.3.3 Wear depth partition factor

Although the wear partition factor in Eq.(19) defines how the total wear volume is distributed between pin and plate, it does not provide an equivalent indication for the proportion between their wear depths, for which numerical simulations are needed. At this purpose another parameter $\tilde{\alpha}$, the wear depth partition factor, can be introduced as the ratio between the maximum wear depth of the cylinder and the sum of maximum wear depths of the two bodies, i.e.

$$\tilde{\alpha}(d)=\frac{h^{\mathrm{c}}_{\max}(d)}{h^{\mathrm{c}}_{\max}(d)+h^{\mathrm{p}}_{\max}(d)}=1-\frac{h^{\mathrm{p}}_{\max}(d)}{h^{\mathrm{c}}_{\max}(d)+h^{\mathrm{p}}_{\max}(d)} \tag{29}$$

It is worth noting that $\tilde{\alpha}$ is a function of the wear cycles (i.e. travelled distance d), while α is a constant input parameter for a given simulation.

The trends of $\tilde{\alpha}$ during the loading history for all the simulated cases are plotted in Fig.13 showing the effect of the stroke amplitude. In case $s_t=a$, $\tilde{\alpha}$ slightly increases or decreases with the travelled distance, depending on α, and assumes an average value very close to α. For instance, for the case $\alpha=0.25$ ($s_t=a$), the percentage variation of $\tilde{\alpha}$ over the travelled distance is 4.5%, with an average value $\bar{\tilde{\alpha}}$ of about 0.266, so that $\bar{\tilde{\alpha}}/\alpha$ is about 1.064. The differences for the other cases $\alpha=0.5$ and $\alpha=0.75$ are even lower, as it can be observed from Fig.13 a). Similar trends are also verified for $s_t=2a$ (Fig.13 b), although the ratio $\bar{\tilde{\alpha}}/\alpha$ is higher than 1, up to 1.30 for $\alpha=0.25$. As the stroke amplitude increases up to s_t,=4a, the trend of $\tilde{\alpha}$ changes markedly (Fig.13 c): firstly, it considerably decreases with d; secondly, $\tilde{\alpha}$ is much higher than α, up to 1.83 times for $\alpha=0.25$. Finally, in the last/extreme case $s_t=2R$, $\tilde{\alpha}$ tends to 1, being higher than 0.96 for any case of α. That is in full agreement with the shape of the worn profiles: the wider the stroke, the deeper the wear scar of the pin (i.e. the higher h^c_{max}) and the flatter the wear groove on the plate surface (i.e. the lower h^p_{max}). In fact, according to Eq. (28), $h^p_{max}(\eta_u)\to 0$ entails $\tilde{\alpha}(\eta_u)\to 1$.

Actually, $s_t=a$ was demonstrated to be a special case for which $\tilde{\alpha}$ is almost constant and can be approximated by α, with an error lower than 8%. Furthermore, in this case, if we consider the wear profiles in the reference configuration, that is when the maximum wear depth of the cylinder and the plate are aligned, the local ratio of the wear depths

$$\tilde{\alpha}_x(x,d)=\frac{h^{\mathrm{c}}(x,d)}{h^{\mathrm{c}}(x,d)+h^{\mathrm{p}}(x,d)} \tag{30}$$

appears nearly equal to $\tilde{\alpha}$ over most of the worn area, Fig.13 e. For instance, Fig.13 e shows the $\tilde{\alpha}_x(x,d_t)$ for $\alpha=0.25$, 0.5, 0.75, highlighting that $\tilde{\alpha}_x$ is uniform and equal to $\tilde{\alpha}$ at the centre of the worn profiles ($-1\leqslant x/a$

⩽1), although a rapid decrease to null value takes place close to the contact edges (x/a <-1 and x/a >1), being the plate worn profile slightly wider than the pin one.

To the purpose of fully investigating how α affects the worn profiles, the sum of the pin and cylinder wear profiles in the reference configuration, i.e.

$$h^{cp}(x,d) = h^{\mathrm{c}}(x,d) + h^{\mathrm{p}}(x,d) \tag{31}$$

was estimated for all simulated cases, as shown in Fig.14. It is interesting to note that, for s_t=a, h^{cp} is not affected by α whilst, as the stroke amplitude increases, the effect of the wear partition factor becomes more and more significant, because the extension of the worn regions becomes different between the bodies, particularly it increases in the plate. Consequently, when s_t=a, the wear partition factor provides a good approximation also of the repartition of the wear depth between the pin and the plate. It can be observed also that, according to Eq.(29), being in this case $\alpha = \tilde{\alpha}$, the following relationship holds:

$$\begin{aligned} h^{\mathrm{c}}_{\max} &= \alpha\left(h^{\mathrm{c}}_{\max} + h^{\mathrm{p}}_{\max}\right) \\ h^{\mathrm{p}}_{\max} &= (1-\alpha)(h^{\mathrm{c}}_{\max} + h^{\mathrm{p}}_{\max}) \end{aligned} \tag{32}$$

where the sum of the wear depths on the right hand does not vary with α. Thus, the value of $h^{\mathrm{c}}_{\max}$ for α=α' is equal to value of $h^{\mathrm{p}}_{\max}$ calculated for α=1-α', as confirmed by the results reported in Fig.11 (e.g. see curves for α=0.25 and α=0.75). However, it is important to underline that this is not true in other cases.

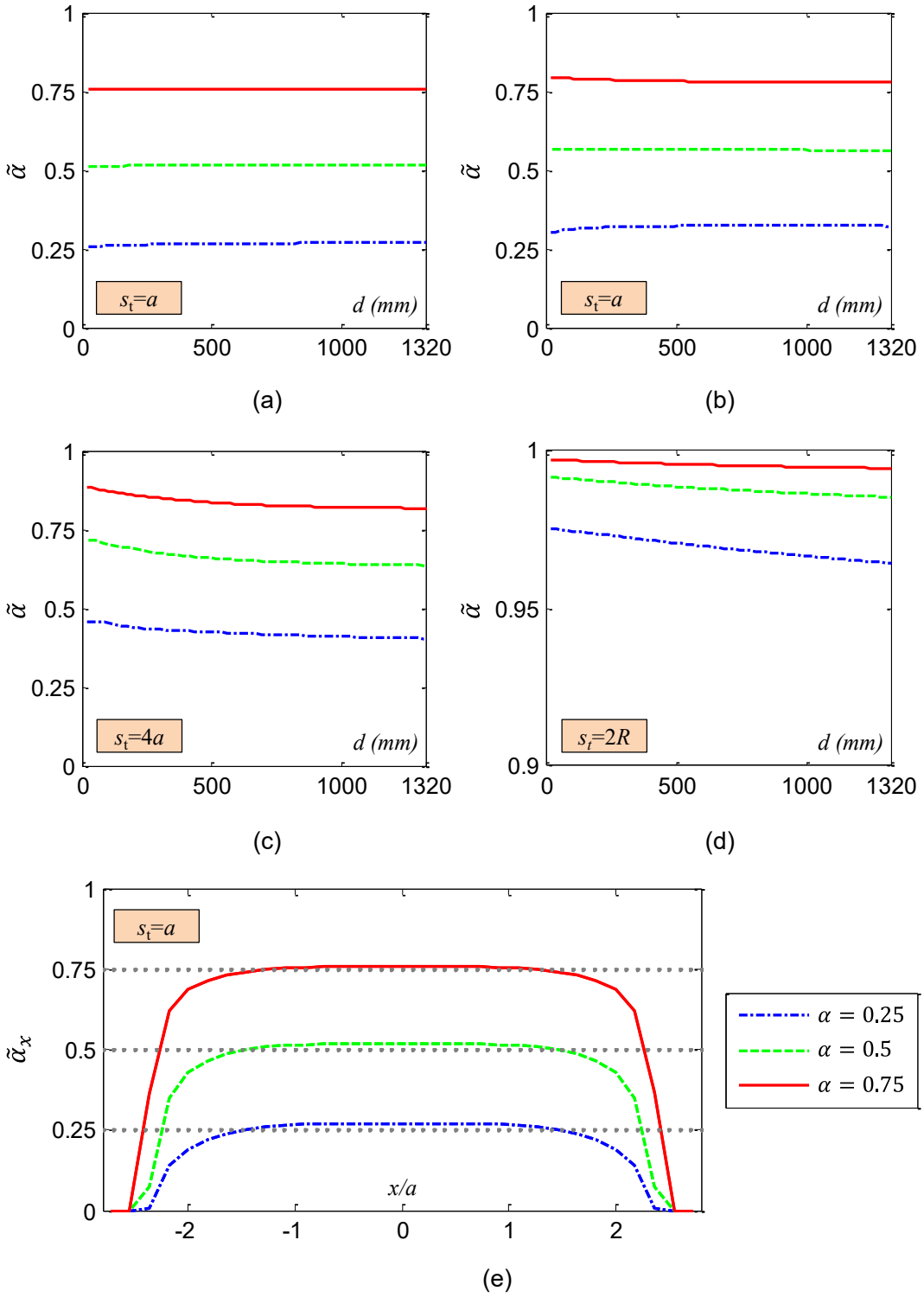

Fig. 13 Wear depth partition factor (Eq.(28)) vs. travelled distance (a-d) (to note the different axis scale for s_t =2R (d))and its local distribution (Eq.(29)) for d_t=1320 mm (e).

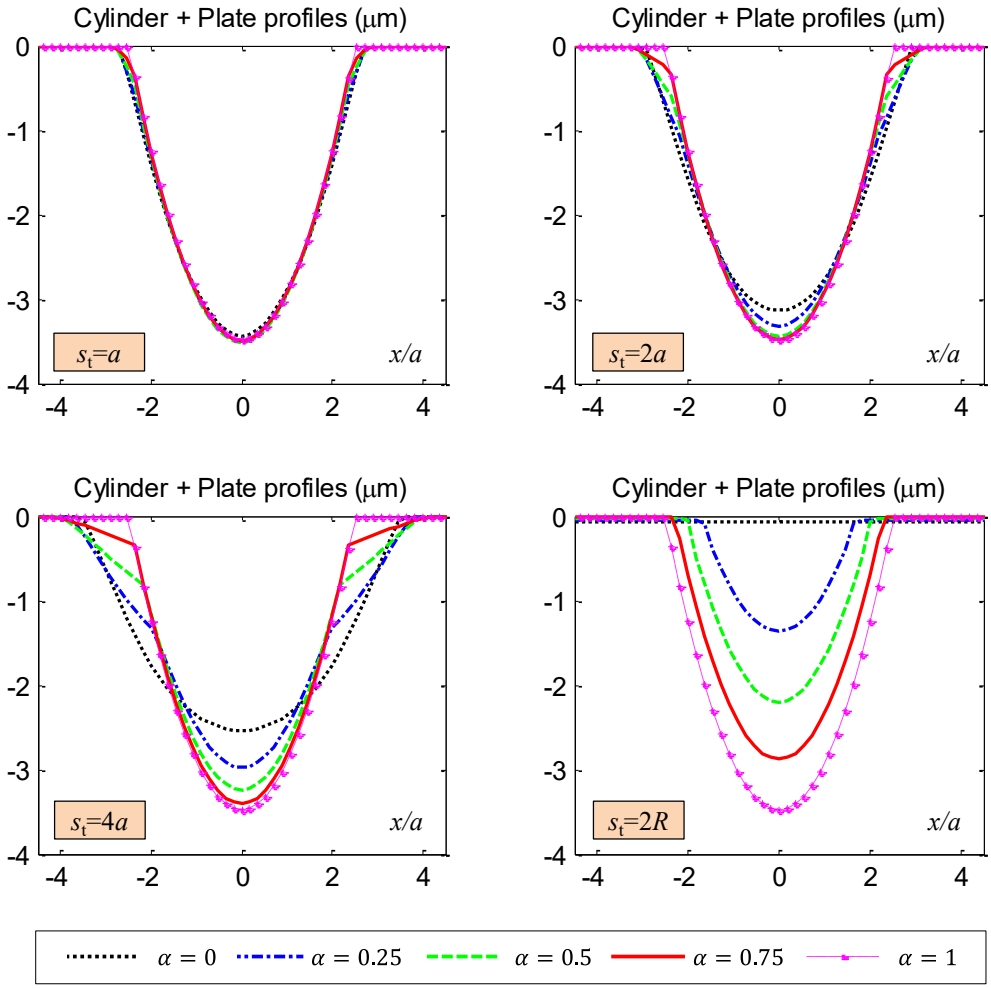

Fig. 84 Sum of the cylinder and plate wear profiles for d_t=1320 mm, in the reference configuration (aligned maximum values), for all the simulated cases.

5.4 Comparison with the literature

A comparison of the presented results with respect to literature is reported in this section. However, it is worth noting that it is complicated by two facts: on the one hand only a few papers are focused on the use of different wear coefficients for the mating surfaces, and, on the other hand, such papers frequently refer to different tribo-systems (i.e. different geometries and BCs) or assume different wear models (e.g. frictional vs frictionless contact, partial slip vs gross slip) with respect to the one described in the present study. Furthermore, as stressed in the introduction, the effect of different wear coefficients is generally not deepened. For instance, an important study in this field was proposed by Mary and Fouvry in 2007 [10], which describes a 2D fretting model of a cylinder-on-plate in gross slip conditions, with friction, under a variable stroke amplitude, lower than the semi-contact width (i.e. s_t<a). The wear model was applied to simulate three different conditions: unilateral wear of the cylinder or of the plate, and bilateral wear, with α=0.5. Results show that, for the latter case, the wear profiles of the pin and the plate are almost identical. Moreover, as the obtained total wear profiles for the three conditions are very similar, (relative difference of the maximum wear depths of 1%), the authors conclude that the simulation of a simple unilateral wear case can be a strategy to reduce the computational costs. That is in very good agreement with our findings for the case s_t=a, thus this result seems not to be affected by the presence of friction.

The two studies by Sfantos and Aliabadi, [16] and [3], also investigate bilateral wear in a pin-on-disc, for the cases k^c= k^p and k^c=2 k^p, using both a 2D and a 3D wear models. However, their simulations are based on some important limiting assumptions. In particular, the 2D model is used to simulate a case where the

sliding occurs orthogonally to the plane (e.g. along z direction in Fig.6) thus considering that the contact area does not to change throughout each wear cycle and nodes in the contact region undergo the same contact pressure and the same sliding distance. Consequently, the pin and the disc have identical worn areas and the resulting wear depths appear to be proportional to the specific wear coefficients. Accordingly, the present study points out that the relationship between the wear partition factor and the wear depth is almost linear in case of very small stroke, holding $\alpha = \tilde{\alpha} = \tilde{\alpha}_x$ for s_t=a. However this is not a general results, as it is not so for higher stroke amplitudes.

As mentioned in the introduction, the only work that has deepened the matter of simulating different wear resistances of the rubbing surfaces was recently proposed by Lengiewicz and Stupkiewicz, [1]. An analytical 3D wear model of a periodic pin-on-flat configuration was developed assuming that the elastic deflections do not influence the contact pressure and the wear process, and it was applied to carry out a sensitivity analysis of wear evolution with respect to a wear mode index, defined as $I_w \propto k^p/(s_t\ k^c)$ (definition revised using the variables of the present study). Unfortunately, a comparison with their results is not possible because, firstly, I_w is varied without specifying the values of each single parameter, and mostly important, the wear coefficients are considered independent one from the other.

As far as the effect of the stroke amplitude is concerned, to the best of our knowledge, only [15] describes a wear model able to simulate both small (i.e. fretting) and large (i.e. sliding) stroke amplitudes. However, different sliding conditions were simulated for different tribo-systems to the purpose of reproducing results available in the literature and validating the model, without deepening the specific effect of the stroke amplitude.

Finally, a brief discussion on the model hypotheses and its limitations is worth being added. First of all, the presented results are based on the assumption of constant values both for k and α. Actually, the wear rate varies throughout the wear process, for example from the running-in to the steady-state wear phase. Consequently it would be important to have experimental measurements of the evolution of the cylinder/pin volume losses to represent the real trend of k and α vs. time/loading cycles that could be easily implemented in our model. Additionally, it is worthnoting that the present study considers the wear factor to be uniform on a contact surfaces. Although this assumption is well accepted for many materials (e.g. steel alloys and ceramics), it does not hold for others ones whose k changes locally on the contact surface. An example is given by ultra high molecular weight polyethylene, a material commonly used in medical prosthesis, whose wear resistance depends from the local re-orientation of the polymeric chains (i.e. cross-shearing effect) [19].

Secondly, the model is based on the simplifying hypothesis of a frictionless contact and thus a gross slip regime. As far as friction is concerned, many literature studies confirmed that its effect on the contact pressure is negligible. On the other hand, the assumption that the effect of the partial slip regime on the overall wear process would be negligibly small is demonstrated by the consistent wear predictions reported in [15] and [2], where identical wear profiles were obtained simulating gross slip regime under frictionless contact and stick-slip conditions under frictional contact (i.e. both partial and gross slip), respectively.

6 Conclusions

The present study describes both procedures and results of the numerical simulations of a two-dimensional wear evolution problem, defined by a cylinder sliding over a plate. The developed procedure has allowed investigating the effect of the wear resistance of the mating surfaces and of the stroke amplitude on the wear process, only marginally treated in the literature.

The paper is organized in order to extensively describe the main aspects, theoretical and numerical, involved in wear simulations. First of all, the Archard wear law, commonly based on one wear coefficient k for the whole coupling, has been generalized to deal with different wear resistances of the rubbing surfaces, thus requiring two distinct wear coefficients k^p and k^c. Such wear coefficients are related to the total one according to the straightforward but fundamental equation k=k^p+k^c. As the concept of wear coefficient is

strictly linked to the coupling, instead of using k^p and k^c, the wear partition factor α is introduced and applied in numerical simulations. Secondly, two basic procedures for wear implementation in Abaqus are described, and the specific solutions adopted in the presented simulations detailed by means of flow charts and equations representing the discretized version of the generalized Archard wear law. In particular, some indications to check the results accuracy while reducing the computational cost are provided. The third aspect is specifically the wear evolution of a cylinder sliding over a plate, and the effect of the stroke amplitude s_t and α on the process, analysed through twenty simulation cases given by the combination of different values of s_t (a, $2a$, $4a$, $2R$) and α (0, 0.25, 0.5, 0.75, 1). The main results obtained from numerical investigations can be summarized as follows

- The load and the total travelled distance being the same in all simulated cases, the total wear volume is the also same, and can be calculated according to the Archard wear law.
- The volume losses of plate and cylinder depend on the value of α and have a linear trend with respect to the travelled distance or loading cycles; in some studies in the literature, it is assessed that linearity holds when geometry does not vary with wear. Our results suggest that it is not so.
- The maximum wear depth of the two profiles have a non linear trend with a decreasing rate as time increases, as contact pressure also decreases as the mating surface become more and more conformal with wear.
- The wear partition factor play a fundamental role on wear evolution and must be included in numerical wear simulations; to this aim, the measurements of separate wear volumes of the contact bodies, though rarely reported in the literature, is needed.
- When the stroke amplitude is comparable to the unworn contact width, i.e. in case of fretting, the wear partition factor provides a reliable indication also of the ratio of the wear depths of the mating surfaces. This means also that the sum of the cylinder and plate wear profiles is constant and does not depend on α. Therefore, the effect of α on the worn profiles, at a given wear cycle, can be easily obtained from a single wear simulation, even from the easiest case of unilateral wear. It should be noted that these observations are not general but related to the examined geometry.
- For a given α, the maximum cylinder wear depth is only slightly affected by the stroke amplitude, while the opposite happens for the plate as the worn region is wider by less depth for higher s_t.
- The effect of α on the contact pressure is more relevant at larger strokes, when indeed higher values of α entail a more conformal contact and uniform pressure distributions. On the other hand, the effect of s_t on the contact pressure is significant for low values of α under which the smaller the stroke, the flatter the pressure distribution.

Some of these points are confirmed by other studies in the literature, although here a wider perspective is provided. In conclusion, although the present study has dealt a simple 2D pin-on-plate configuration, it introduces in every detail the simulation of wear evolution with a partition factor, providing a tool that can be rather easily applied to three dimensional problems as well.

7 Bibliography

[1] J. Lengiewicz, S. Stupkiewicz, Efficient model of evolution of wear in quasi-steady-state sliding contacts, Wear, 303 (2013) 611-621.
[2] I.R. McColl, J. Ding, S.B. Leen, Finite element simulation and experimental validation of fretting wear, Wear, 256 (2004) 1114-1127.
[3] G.K. Sfantos, M.H. Aliabadi, A boundary element formulation for three-dimensional sliding wear simulation, Wear, 262 (2007) 672-683.
[4] J. Andersson, A. Almqvist, R. Larsson, Numerical simulation of a wear experiment, Wear, 271 (2011) 2947-2952.
[5] Z.M. Jin, P. Firkins, R. Farrar, J. Fisher, Analysis and modelling of wear of cobalt-chrome alloys in a pin-on-plate test for a metal-on-metal total hip replacement, Proc Inst Mech Eng H, 214 (2000) 559-568.
[6] N.H. Kim, D.K. Won, D. Burris, B. Holtkamp, G.R. Gessel, P. Swanson, W.G. Sawyer, Finite element analysis and experiments of metal/metal wear in oscillatory contacts, Wear, 258 (2005) 1787-1793.

[7] A. Rezaei, W. Van Paepegem, P. De Baets, W. Ost, J. Degrieck, Adaptive finite element simulation of wear evolution in radial sliding bearings, Wear, 296 (2012) 660-671.
[8] F.J. Martinez, M. Canales, S. Izquierdo, M.A. Jimenez, M.A. Martinez, Finite element implementation and validation of wear modelling in sliding polymer-metal contacts, Wear, 284 (2012) 52-64.
[9] E.M. Bortoleto, A.C. Rovani, V. Seriacopi, F.J. Profito, D.C. Zachariadis, I.F. Machado, A. Sinatora, R.M. Souza, Experimental and numerical analysis of dry contact in the pin on disc test, Wear, 301 (2013) 19-26.
[10] C. Mary, S. Fouvry, Numerical prediction of fretting contact durability using energy wear approach: Optimisation of finite-element model, Wear, 263 (2007) 444-450.
[11] M. Oqvist, Numerical simulations of mild wear using updated geometry with different step size approaches, Wear, 249 (2001) 6-11.
[12] G.X. Chen, Z.R. Zhou, Study on transition between fretting and reciprocating sliding wear, Wear, 250 (2001) 665-672.
[13] S. Heredia, S. Fouvry, Introduction of a new sliding regime criterion to quantify partial, mixed and gross slip fretting regimes: Correlation with wear and cracking processes, Wear, 269 (2010) 515-524.
[14] P. Podra, S. Andersson, Simulating sliding wear with finite element method, Tribol Int, 32 (1999) 71-81.
[15] I. Argatov, W. Tato, Asymptotic modeling of reciprocating sliding wear - Comparison with finite-element simulations, Eur J Mech a-Solid, 34 (2012) 1-11.
[16] G.K. Sfantos, M.H. Aliabadi, Wear simulation using an incremental sliding Boundary Element Method, Wear, 260 (2006) 1119-1128.
[17] K.W. Man, M.H. Aliabadi, D.P. Rooke, Bem Frictional Contact Analysis - Modeling Considerations, Eng Anal Bound Elem, 11 (1993) 77-85.
[18] K.L. Johnson, Contact Mechanics, Cambridge University Press, Cambridge, 2001.
[19] L. Mattei, F. Di Puccio, E. Ciulli, A comparative study on wear laws for soft-on-hard hip implants using a mathematical wear model, Tribol Int, 63 (2013) 66-77.